MRC/ABQ-R-1391
Copy ___/___

Mission Research Corporation

PHERMEX, REX, AND THOMSON-GENERATED XUV CALCULATIONS

Annual Report

Thomas P. Hughes
Randy M. Clark
Mission Research Corporation

Randolph L. Carlson
David C. Moir
Los Alamos National Laboratory

April 1991

Prepared for: LOS ALAMOS NATIONAL LABORATORY
Post Office Box 1663
Los Alamos, NM 87545

Under Contract: 9-X60-G2910-1

Prepared by: MISSION RESEARCH CORPORATION
1720 Randolph Road, SE.
Albuquerque, NM 87106–4245
(505) 768-7600

DISCLAIMER

ACKNOWLEDGEMENTS

Assistance in modifying and running the XLR8R code was provided by D. Mitrovich. The cathode design in Fig. 2 was obtained from M. Burns and J. Ruhe. The magnet design in Fig. 19 is by M. Burns. M. Menzel provided the version of POISSON needed to produce the results in Fig. 19.

CONTENTS

FIGURES

FIGURES (Continued)

FIGURES (Concluded)

1.0 INTRODUCTION

We report on calculations carried out during 1990 in support of on-going and planned beam experiments at M-4. A higher-current injector for PHERMEX is under consideration and we have modeled a REX-like diode geometry which can deliver 1–1.5 kA. A three-coil focusing configuration has been designed to maintain low beam emittance in the diode region. We show that the existing two transport magnets are marginally capable of transporting a 1 kA beam to the α-cavity. This work is described in Sec. 2. In Sec. 3, we look at the possibility of accelerating a 4 kA, 4 MV beam, which could be provided by the REX machine, through the PHERMEX α cavity. Simulation results indicate that this is feasible. Because of the high cost and limited pulse length of a REX injector, however, a 1–1.5 kA upgrade is a more attractive option at this time. Computations in support of ongoing REX experiments are described in Sec. 4. We have modeled the generation of transverse beam oscillations through the excitation of an electromagnetic dipole mode in the diode cavity. Results show that oscillating magnetic fields on the order of 1–2 gauss are sufficient to cause the oscillation amplitudes observed. A simulation was carried to look at the effect of placing iron rings inside the windings of the REX anode magnet. We conclude that this causes no significant degradation of beam emittance. We have also looked at the focusing produced when the REX beam is injected into a laser-ionized plasma channel. This is a possible alternative to a magnetic lens to obtain a small spot-size. Finally, in Sec. 5, we give results of preliminary calculations of XUV and X-ray photon production through laser backscattering off a relativistic electron beam. There are plans to carry out such an experiment on REX in the near future.

2.0 PHERMEX DIODE UPGRADE

The nominal beam parameters produced by the Pierce diode on PHERMEX are 500 A at 600 kV. It is not practical to increase the beam current by raising the applied voltage because of the likelihood of surface breakdown of the focusing electrode. To avoid this problem, we have investigated using a REX-type diode, with a flat emission surface on a flat electrode. This allows the stress on the emission surface to be significantly increased without breakdown of the surrounding electrode. Since one is giving up the electrostatic focusing of the Pierce geometry, a magnet is required to capture the beam as it enters the anode.

Our attention focused on two designs with nominal parameters of 1.5 kA at 600 kV, and 1 kA at 750 kV. Exact parameters are given in Table 1.

TABLE 1. Upgraded PHERMEX diode parameters

	(a)	(b)
Beam Current (kA)	1.46	1.08
Applied Voltage (kV)	602	750
AK gap (cm)	7.5	7.5
Emission radius (cm)	5.125	3.625
Emittance at 40 cm (cm-rad)		
Two-coil design	0.14	—
Three-coil design	0.042	0.02
Run Identifier	AQ6	AW

Initial calculations were carried out for a 1.5 kA, 600 kV diode with a coil configuration consisting of a focusing solenoid inside the reentrant anode and a bucking coil in the plane of the cathode surface. The bucking coil was adjusted to zero out the axial field at the edge of the cathode. This configuration gave the results in Fig. 1. The cathode temperature was set to zero, so that the emittance is zero at the cathode surface. The rather large emittance of 0.14 cm-rad at 40 cm from the cathode is due to the radial nonlinearity of the magnet focusing. To reduce this effect, we introduced a third coil with radius smaller

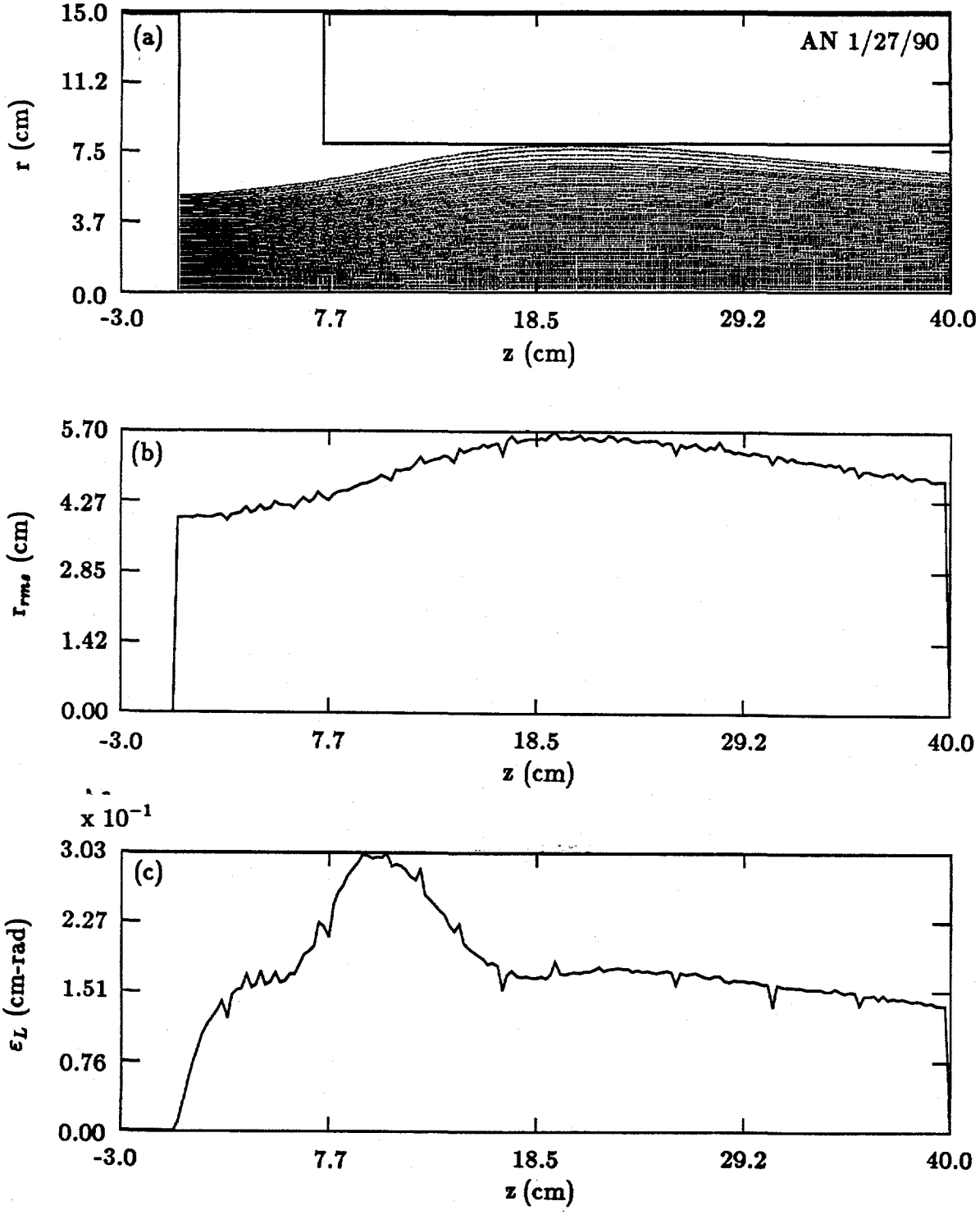

Figure 1. Simulation of proposed PHERMEX diode with two-coil focusing scheme. Particle plot is shown in (a), *rms* radius vs. z is in (b), and emittance vs. z is in (c). (Run AN3, $I_b = 1.46$ kA, $V = 602$ kV).

than, and carrying current in the opposite direction to, the focusing solenoid. This coil reduces the focusing nonlinearity. It is most effective when placed at the location where the beam radius is largest. The coil configuration is shown in Fig. 2, and the improvement in beam emittance can be seen in Fig. 3.

The next step was to transport this beam to the PHERMEX α-cavity. In the present PHERMEX machine, the distance from the cathode to the α-cavity entrance is about 1.57 m, and two iron-clad magnets are used to focus the beam (see Ref. 1, p. 201). We assumed that this distance would remain unchanged for the upgraded diode. Using the code POISSON,[2] we computed the axial magnetic fields for the two iron magnets. This, together with beam data from the simulation in Fig. 3, was used in an envelope model of the beam transport. It was quickly apparent that the fields from the iron magnets were too localized for good transport of the high-current beam. To widen the fields, the iron shielding was removed from the inner radius of the magnets, and the field profile was recalculated. This allowed the beam to be transported about 1.2 m, as shown in Fig. 4. To take the beam further, an additional magnet would be needed. As a check on the envelope model and to observe emittance behavior, we did a particle simulation out to $z = 1$ m. The results in Fig. 5 are in agreement with the envelope code. The emittance, which is assumed constant in the envelope code, is seen to oscillate due to the variations in the radial magnetic field profile, $B_z(r)$. This does not have a significant effect on the *rms* radius, since space-charge is the dominant defocusing term.

For a 1 kA beam at 750 kV, the beam can be transported further using just two magnets because of the lower perveance. The envelope result in Fig. 6 shows that it is possible to reach $z \approx 150$ cm before the beam starts to expand. This is confirmed by the particle simulation in Fig. 7. Our conclusion is that two magnets are only marginally sufficient to transport the beam to the α-cavity. A third magnet would give considerably more flexibility.

Our studies to date have not looked at the effect of diode voltage fluctuations on the downstream transport. This needs to be addressed before a final magnet design is chosen.

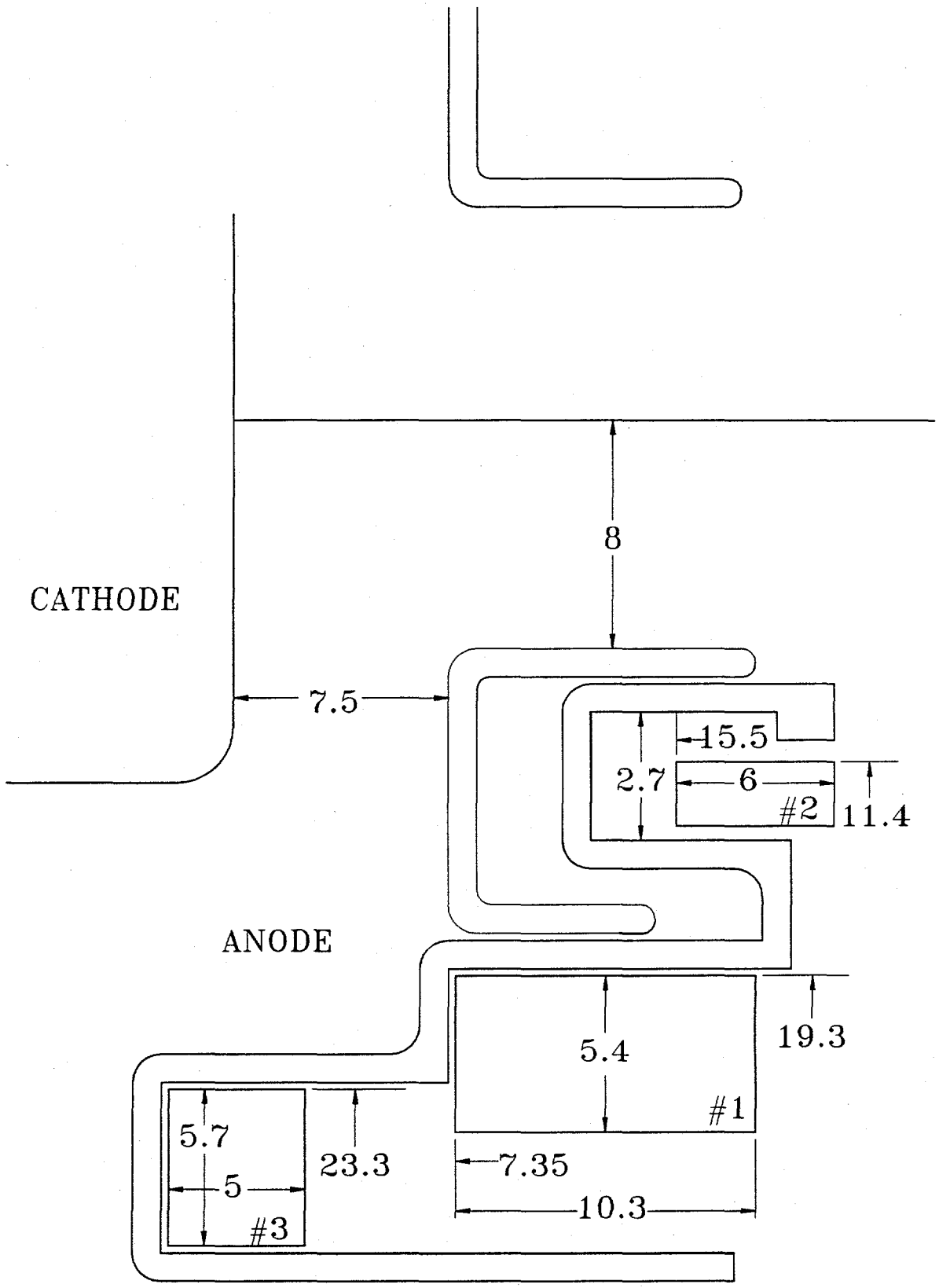

Figure 2. A three-coil configuration used to improve linearity of focusing in diode region. For case in Fig. 3, Coil 1 has 36 kA-turns, coil 2 has -5 kA-turns, and coil 3 has 25.5 kA-turns. (Drawing by M. Burns and J. Ruhe).

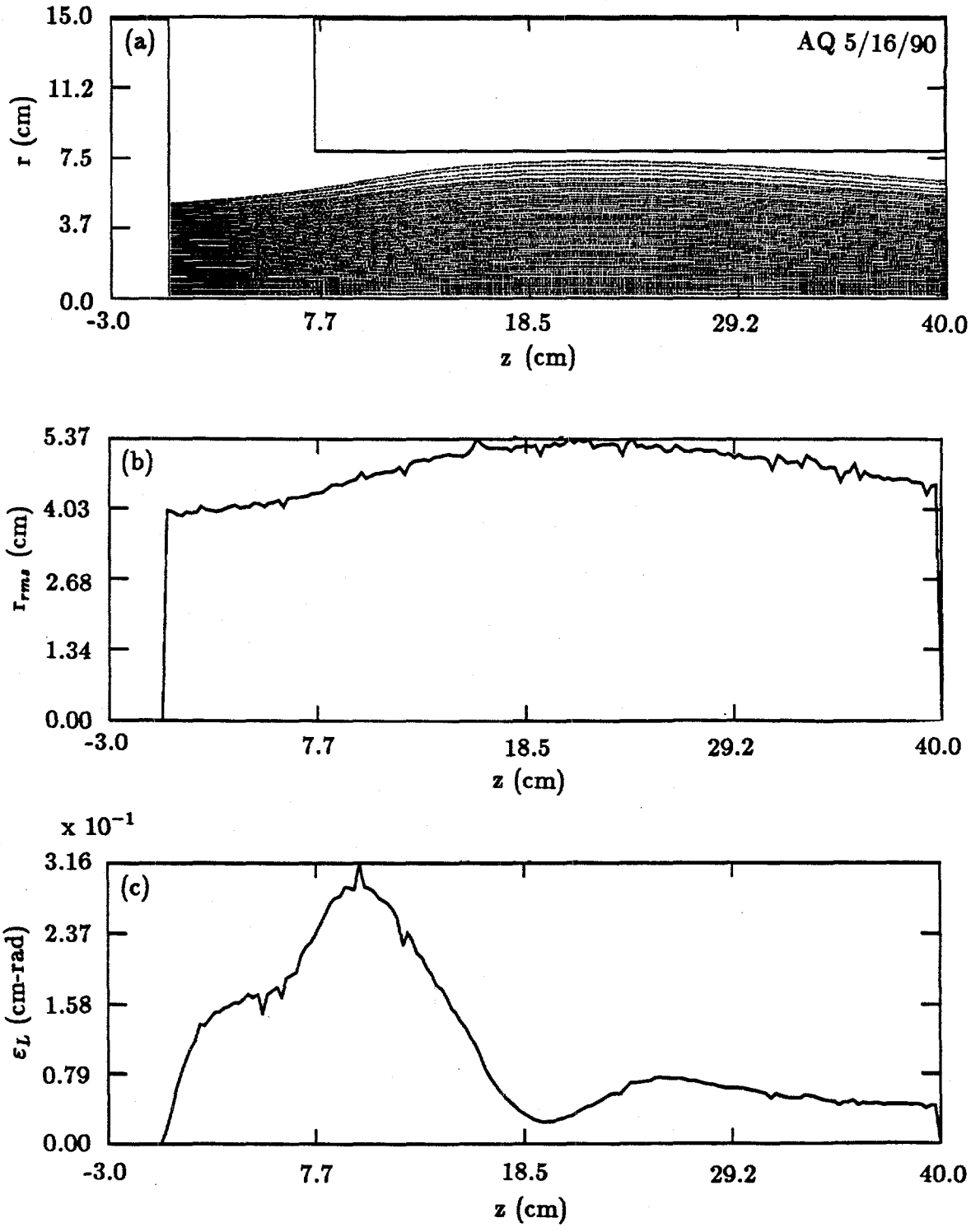

Figure 3. PHERMEX diode simulation with three-coil configuration in Fig. 2. Particle plot is shown in (a), *rms* radius vs. z is in (b), and emittance vs. z is in (c). (AQ6, I_b = 1.46 kA, V = 602 kV). Note the improvement in beam emittance over Fig. 1.

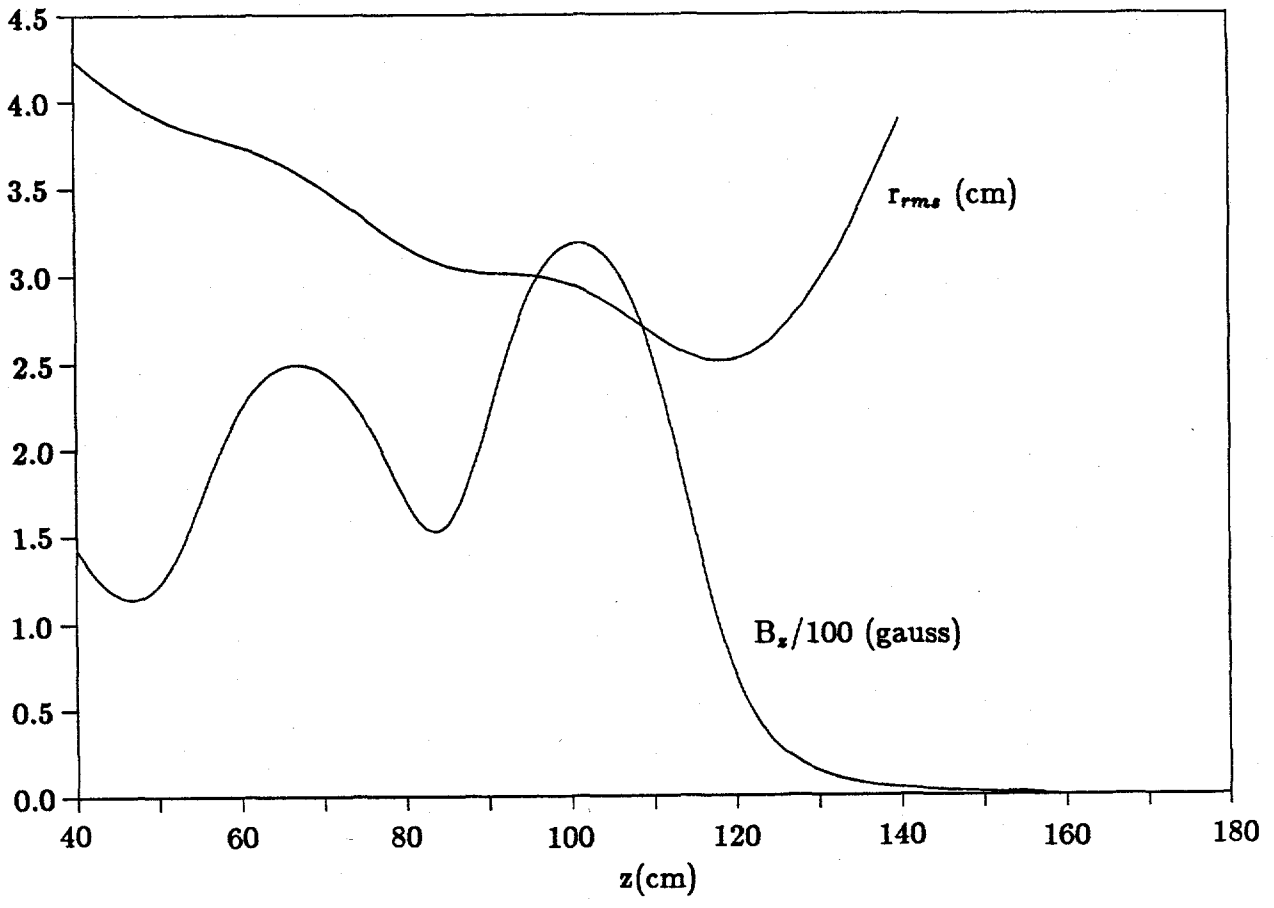

Figure 4. Envelope code simulation of transport through two iron-shield magnets for 1.46 kA, 602 kV beam. Magnet centers are at 67.5 and 101.5 cm from cathode surface.

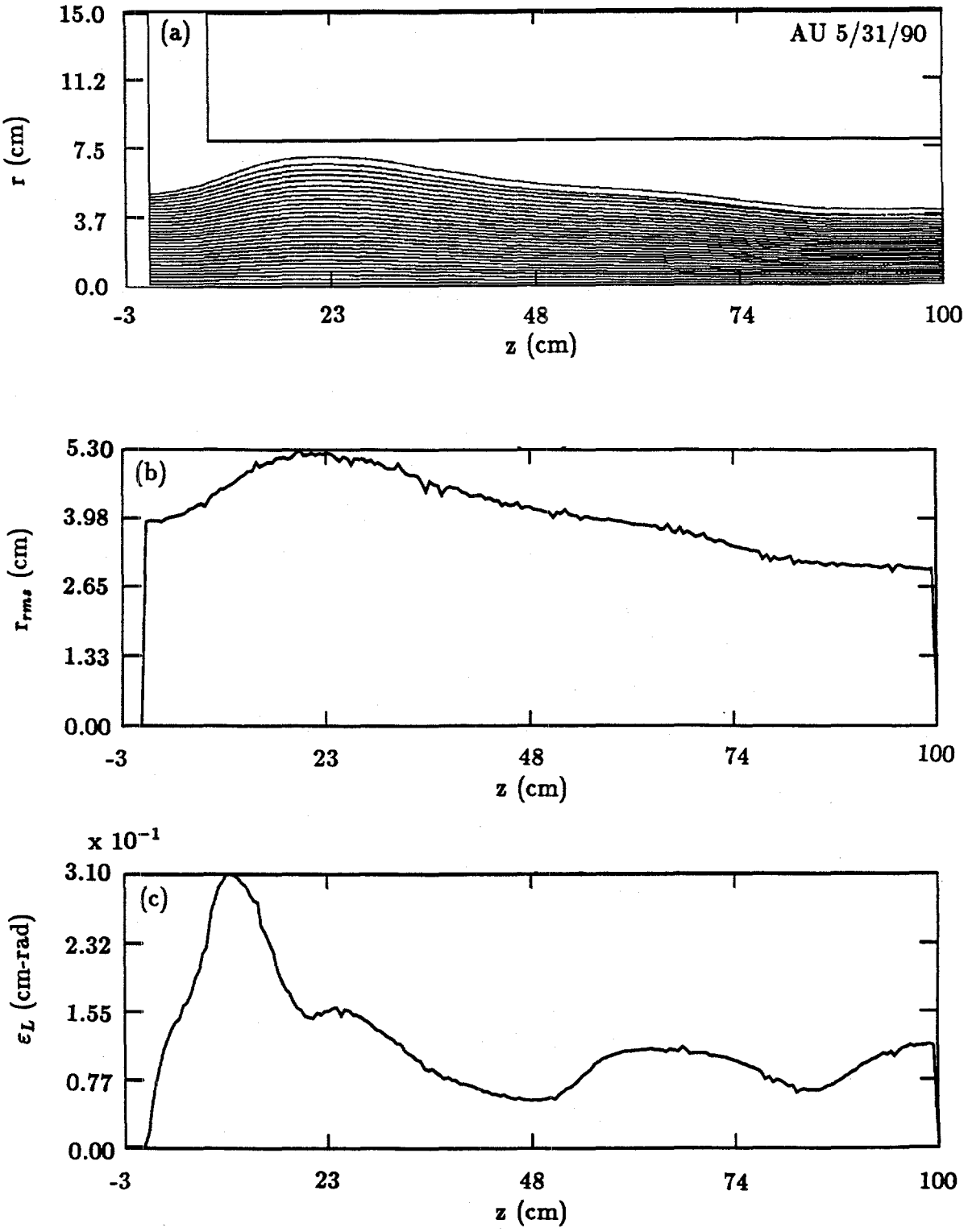

Figure 5. Particle simulation of beam transport from cathode surface through anode magnet and two iron-shield magnets. Iron magnets have same configuration as in Fig. 4. Particle plot is shown in (a), *rms* radius vs. z is in (b), and emittance vs. z is in (c). (Run AU, $I_b = 1.46$ kA, $V = 602$ kV).

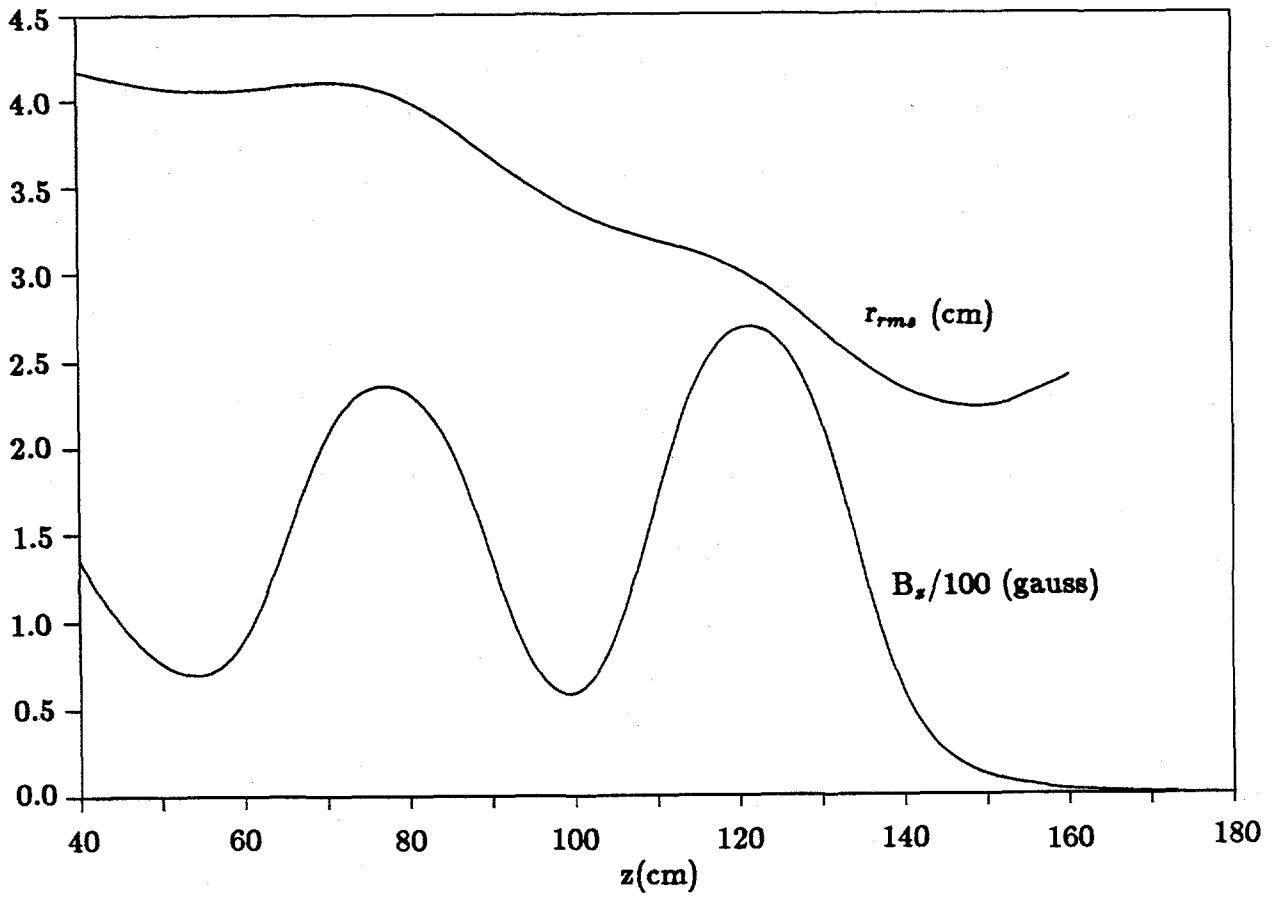

Figure 6. Envelope code simulation of transport through two iron-shield magnets for 1 kA, 750 kV beam. Magnet centers are at 77.5 and 121.5 cm from cathode surface.

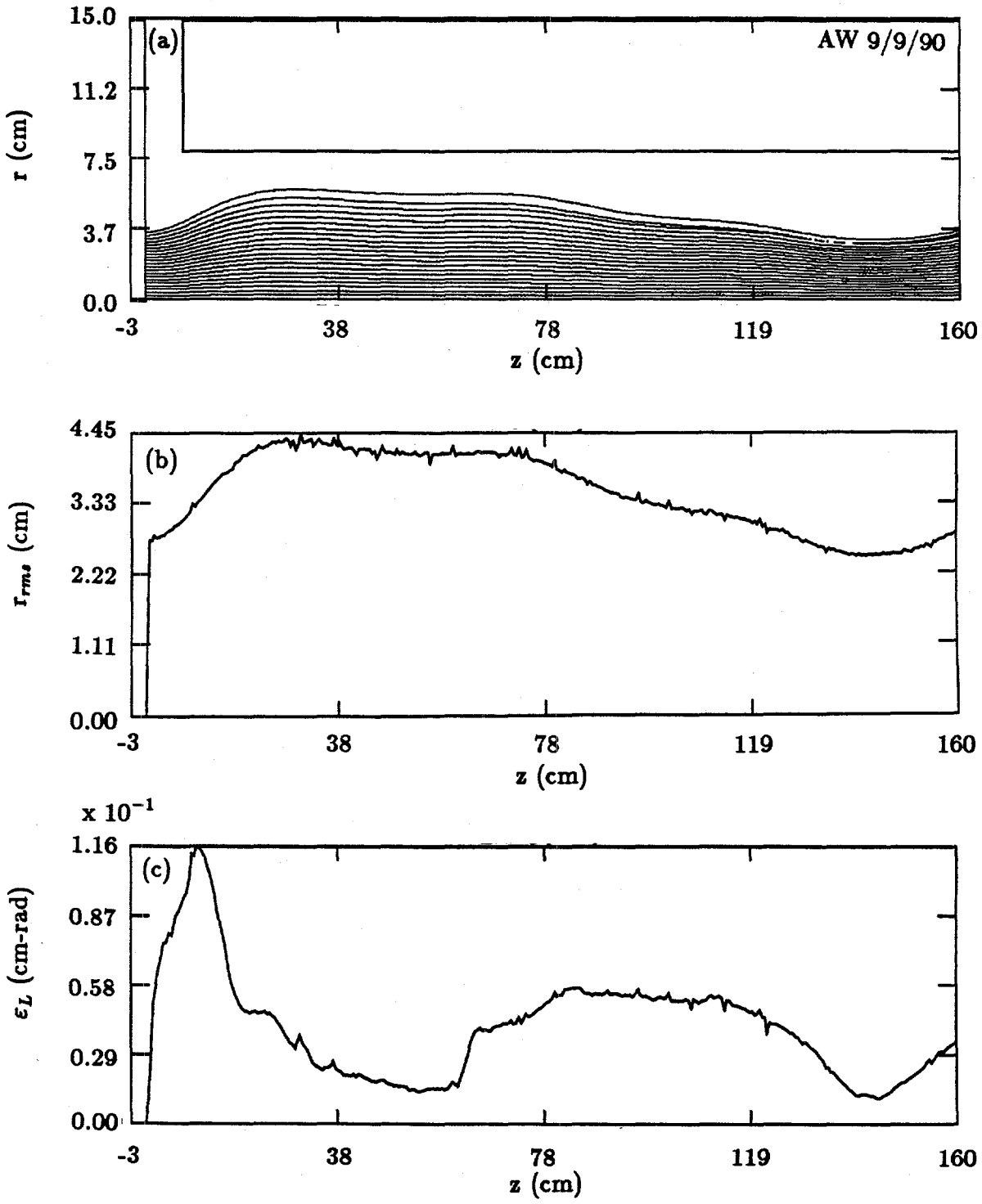

Figure 7. Particle simulation of transport for 1 kA, 750 kV beam. Iron magnets have same configuration as in Fig. 6. Particle plot is shown in (a), *rms* radius vs. z is in (b), and emittance vs. z is in (c). (Run AW, $I_b = 1.08$ kA, $V = 750$ kV).

3.0 HIGH CURRENT BEAM ACCELERATION IN PHERMEX α-CAVITY

In considering possible upgrades of the PHERMEX machine, the question arose whether one could transport and accelerate a beam of several kA, such as that produced by REX, through the PHERMEX rf cavities. If successful, such a beam could result in a significantly higher radiation dose than the present machine. To investigate this, we made preliminary calculations using the code XLR8R,[3] which is a beam envelope model of the PHERMEX accelerator from the α-cavity through to the final aperture. We used the nominal parameters in Table 2. The results in Fig. 8a show that for a 4 kA, 4 MV injected beam, a 4 kA, 30 MV micropulse of width 2.9 ns is transported through the final aperture of 1 cm diameter. The charge through this aperture is 13.5 μC. A similar calculation for the present nominal injection parameters of 500 A and 600 kV, results of which are shown in Fig. 9, gives a charge of 0.9 μC, fifteen times less, through the final aperture.

TABLE 2. Nominal parameters for REX beam transport in PHERMEX

Beam Current (kA)	4
Beam Injection Energy (MV)	4
Injection Radius (cm)	4
Accelerating Fields (MV/m):	
α Cavity	6
β Cavity	5
γ Cavity	4
Phase Differences: $\alpha - \beta$	193°
$\beta - \gamma$	193°

The present PHERMEX injector produces a 200 ns beam pulse, which gives a train of ten micropulses, since the period of the PHERMEX rf is 20 ns. Thus, according to these calculations, a single 4 kA micropulse contains more charge than ten 500 A micropulses. For a pulsed power injector like the present REX machine, the beam pulse length is on the order of 70 ns, so that one could generate up to 4 micropulses. If each micropulse is similar to that in Fig. 8, then the total charge going through the final aperture is estimated to be 54 μC, or about 6 times more than for a stream of ten 500 A pulses.

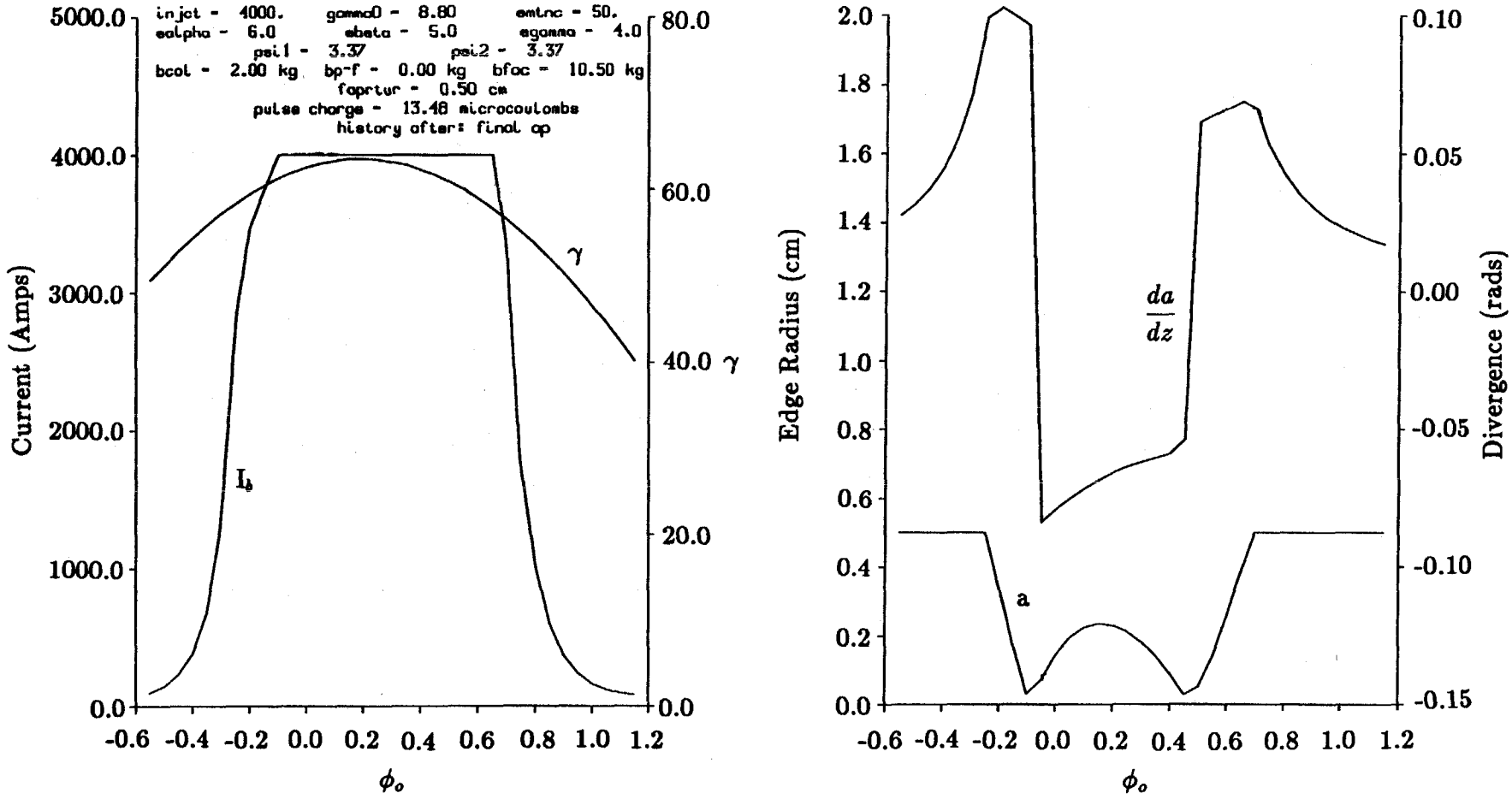

Figure 8. XLR8R results for 4 MV, 4 kA beam at final aperture in PHERMEX. Beam current and γ are plotted vs. injected phase angle in (a). Beam radius and divergence angle are plotted vs. injected phase angle in (b).

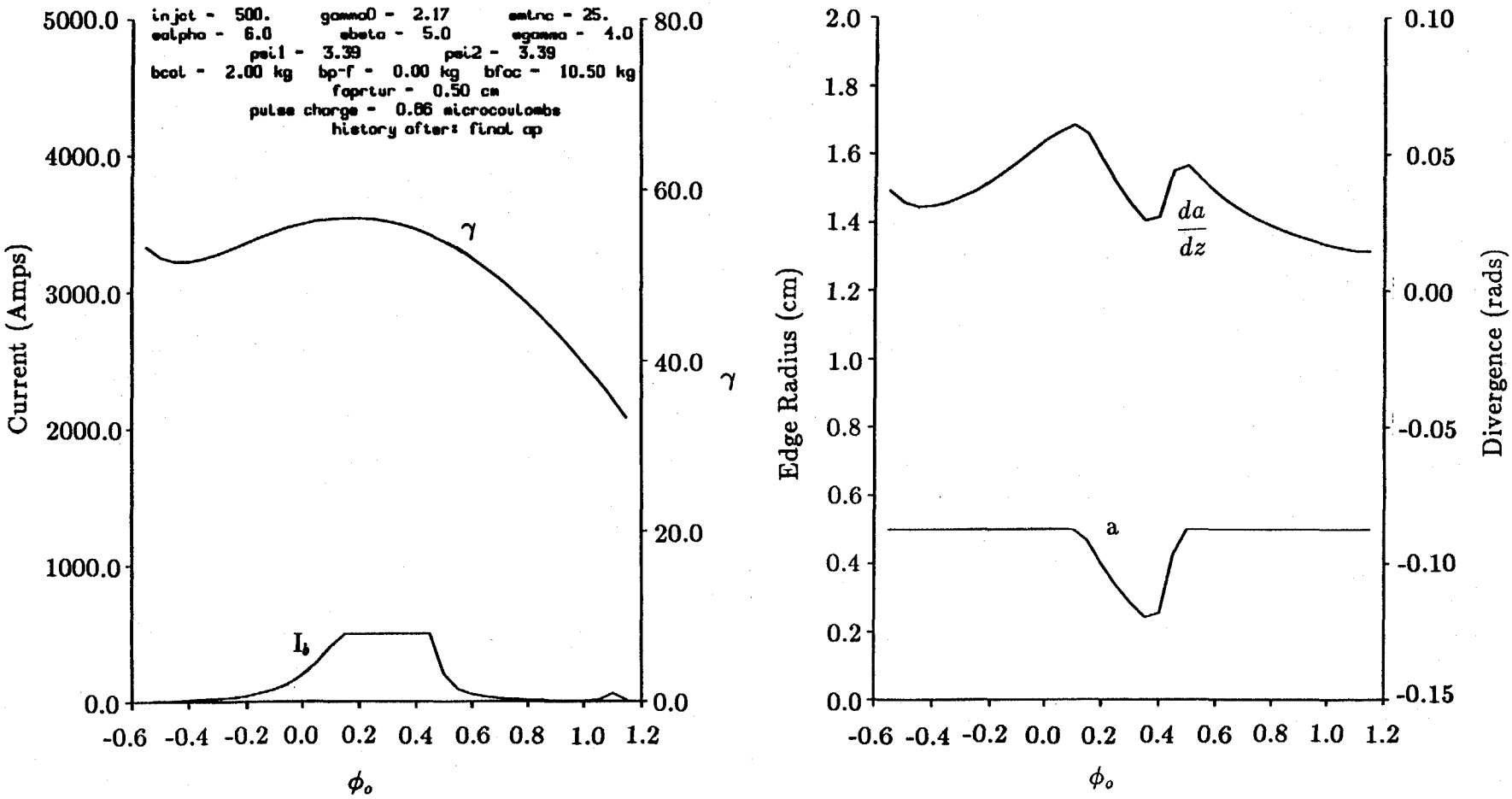

Figure 9. XLR8R results for 600 kV, 500 A beam at final aperture. Beam current and γ are plotted vs. injected phase angle in (a). Beam radius and divergence angle are plotted vs. injected phase angle in (b).

A potential problem with this scenario is the energy depletion of the rf cavities as pulses are accelerated. The resulting energy dispersion on the beam could make it impossible to obtain a small spot size for each micropulse. We can estimate the energy depletion by calculating the energy gained by an accelerated beam pulse. Assuming the accelerating field is of the form $E_z(t) = -E_0 \sin(\omega_0 t)$, then a particle exiting the cavity at time t has experienced a voltage $V(t)$ given by

$$\begin{aligned} V(t) &= \int_0^L E_z\left(t + \frac{z-L}{c}\right) dz \\ &= \frac{cA}{\omega_0} \cos\left(\omega_0 t + \phi\right) \end{aligned}$$

where

$$A = E_0 \sqrt{\left(1 - \cos\frac{\omega_0 L}{c}\right)^2 + \sin^2\frac{\omega_0 L}{c}}$$

$$\tan\phi = \frac{\sin\frac{\omega_0 L}{c}}{1 - \cos\frac{\omega_0 L}{c}} \tag{1}$$

and where L is the length of the cavity, and we have assumed that the particle is moving with velocity $v_z \approx c$. If one injects a pulse of length τ and current I_b, then the energy absorbed by the pulse is

$$\Delta E = \frac{2cAI_b}{\omega_0^2} \sin\frac{\omega_0 \tau}{2} \cos\left(\phi + \omega_0 t_c\right) \tag{2}$$

where t_c is the time at which the center of the pulse exits the cavity. This derivation neglects energy lost by the pulse (energy gained by the cavity) in exciting higher-order modes (HOM's) in the cavity. It also does not treat the case of continuous beam injection, where a substantial fraction of the beam does not make it across the cavity. To include these effects, we simulated beam transport through the PHERMEX α-cavity using IVORY for both continuous and chopped beam injection. Results for continuous injection over two rf periods are shown in Figs. 10–12. Figure 10 is a sequence of snapshots of beam particle

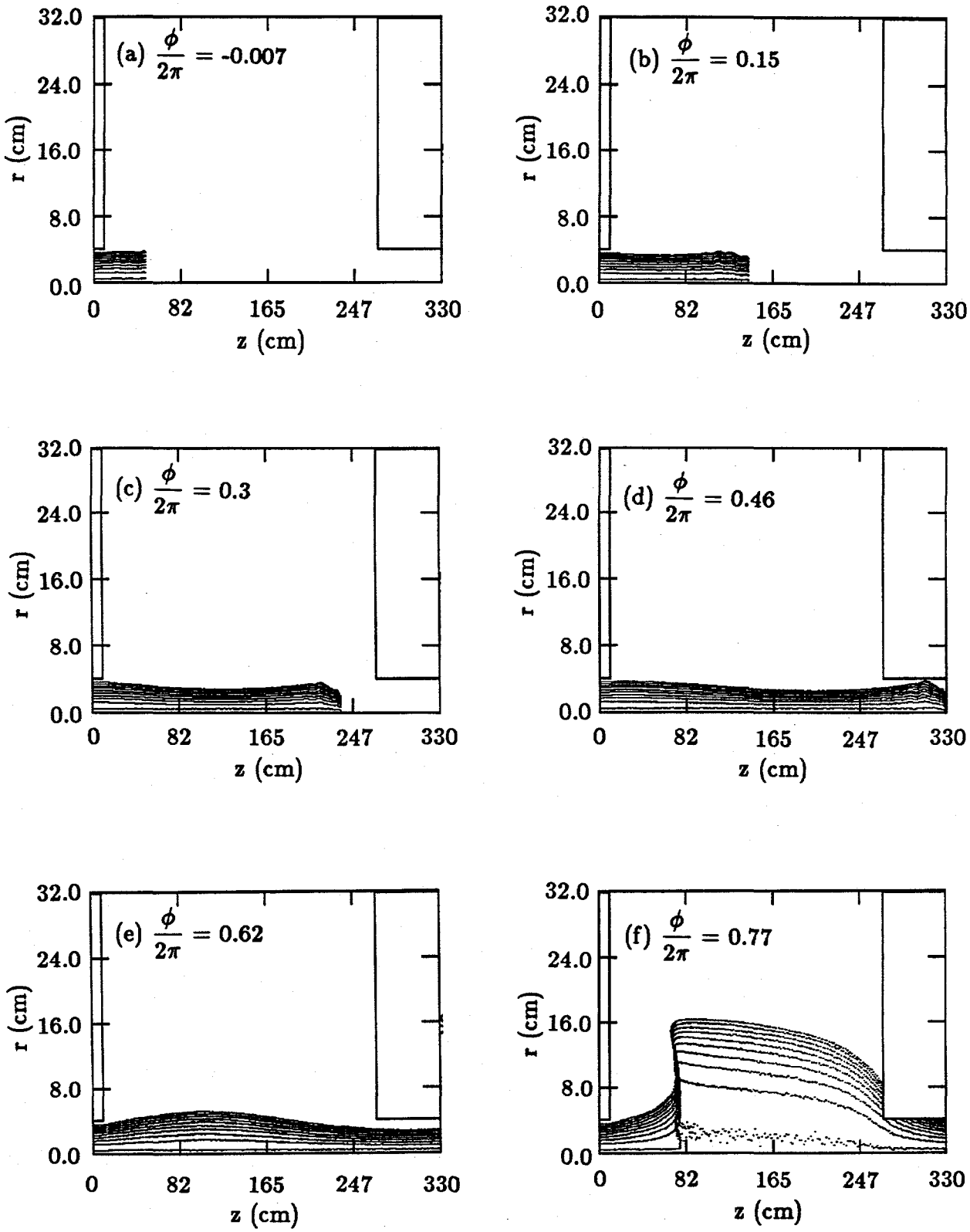

Figure 10. Particle plots over two rf periods of continuous injection of 4 MV, 4 kA beam into PHERMEX α-cavity. The phases, $\phi(t)$, assume $E_z = -E_0 \sin(\phi(t))$. (Run AE, 12/28/90)

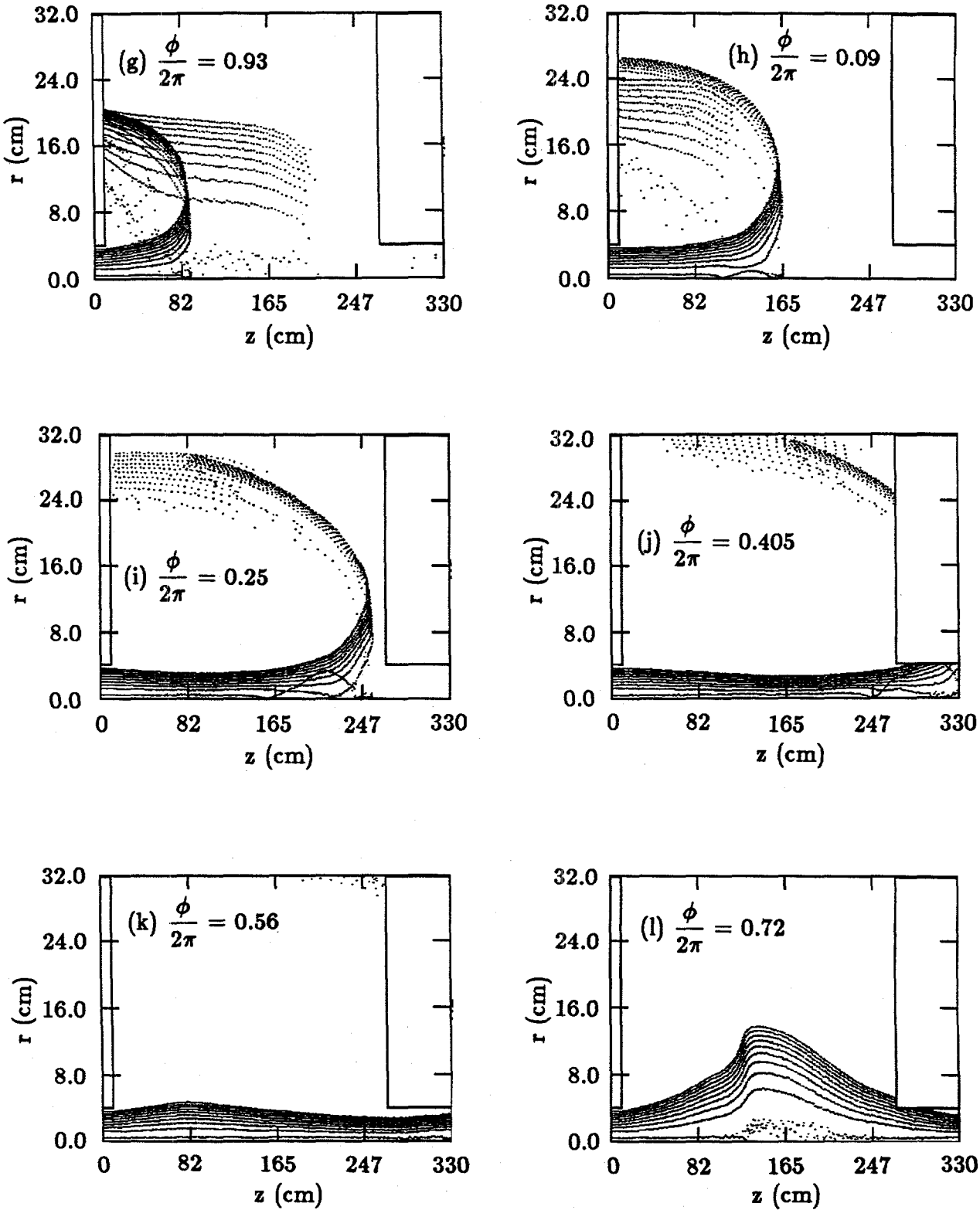

Figure 10. Concluded.

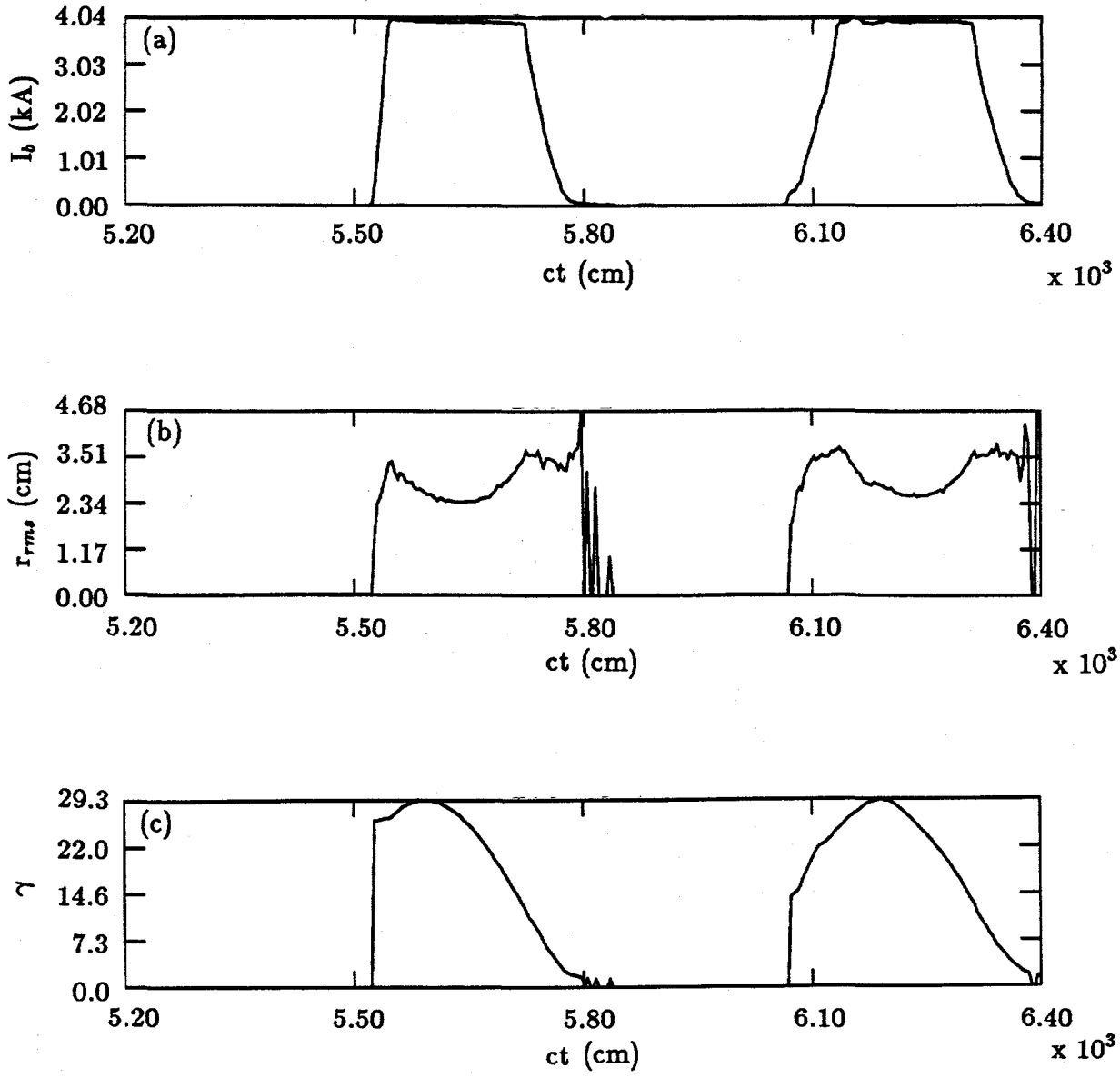

Figure 11. Time histories of (a) beam current, (b) *rms* radius and (c) energy (γ) at the exit of the α cavity for continuous beam injection. (Run AE).

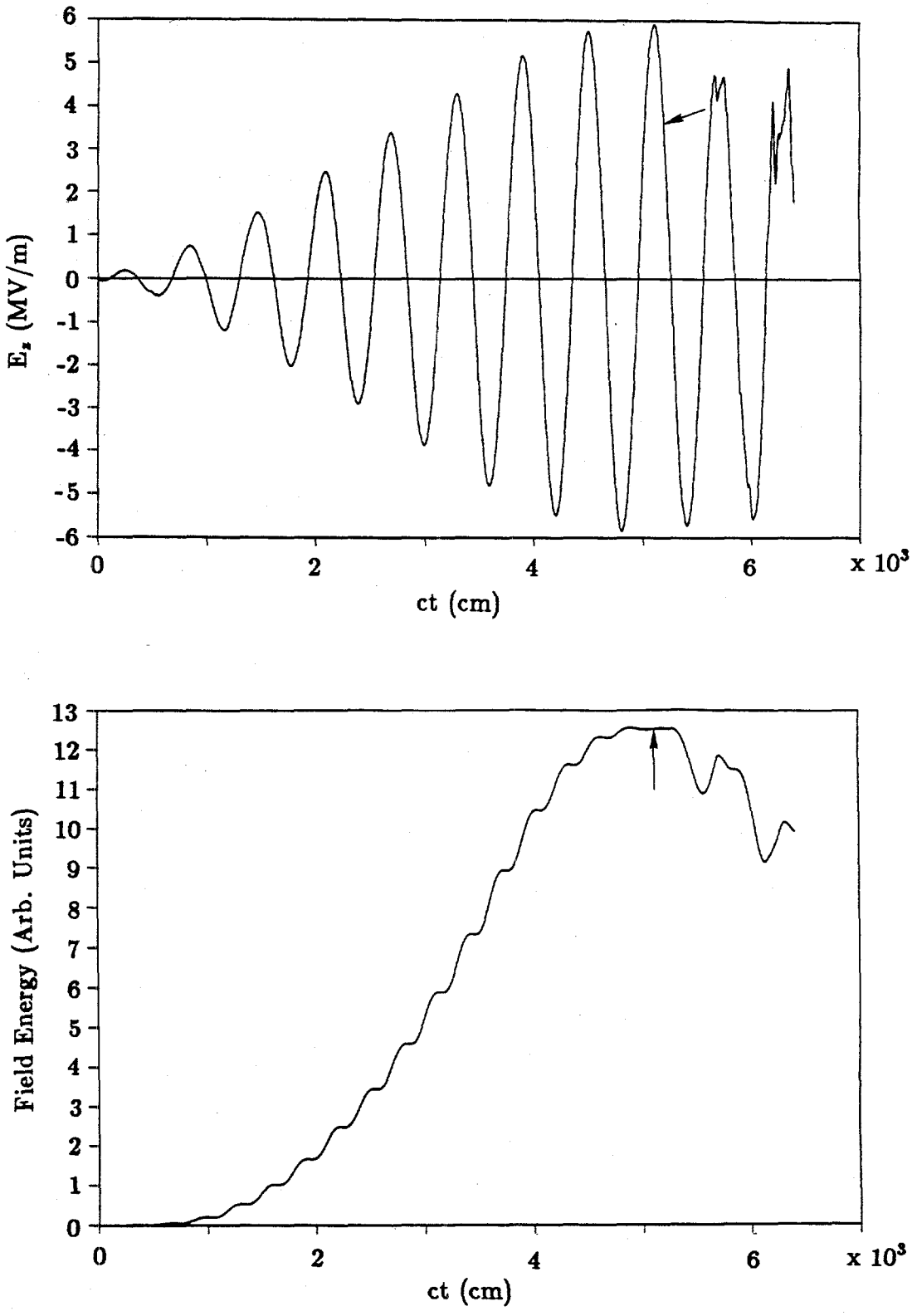

Figure 12. Time histories of (a) axial electric field in center of cavity and (b) cavity field energy for continuous beam injection. The start of injection is indicated by an arrow (Run AE).

positions over the two periods. The current, *rms* radius and particle energy plots in Fig. 11 show that the two micropulses are quite similar at the exit of the cavity. The width of the pulses at peak current is about 6 ns. The electric field history in Fig. 12a samples E_z at the center of the cavity. To initialize the simulation, the cavity is pumped up over about 8 rf cycles using artificial currents until the field amplitude is about 6 MV/m. The artificial currents are then turned off and the beam is injected. The field energy in Fig. 12b shows oscillations superimposed on a secular drop after beam injection. The oscillations are believed to be primarily due to energy exchange with particles which do not get across the cavity. Prior to beam injection, the total field energy in the cavity is about 1.8 kJ. The energy drops by 140 J after the first pulse, and by an additional 230 J after the second pulse. The large difference between the two pulses is probably due to the work done on beam particles which accumulate in the cavity during the deceleration cycle (see frames (g)–(j) in Fig. 10).

In the case of a chopped beam, injection is timed to occur so that particles are near the peak of the accelerating voltage. Results for two consecutive 6 ns pulses are shown in Figs. 13–15. Figure 14 shows that the two exiting pulses are quite similar, although a drop in the peak energy is visible. From Fig. 14a, we find that the pulses are clipped to about 5 ns by the exiting aperture. From Figs. 14b and 14c, we see that the point of minimum *rms* radius lags the point of peak energy. This is because the accelerating rf fields are radially focusing, and particles entering the cavity at the start of the accelerating cycle experience less focusing near the point of injection than particles entering later. The field history in Fig. 15a is less noisy than that in Fig. 12a because of the absence of decelerating particles. From the energy history in Fig 15b, we find that 165 J and 172 J are extracted by the first and second pulse, respectively. (The second pulse is slightly longer than the first pulse.) Since the pulses have a well-defined length, we can compare these values with the estimates from Eq. 2. This expression predicts that the first and second pulses should absorb about 169 J and 171 J, respectively, in good agreement. This suggests that the amount of energy energy deposited in HOM's is small. The pulses in Fig. 14 are injected about 2.1 ns too late in the rf cycle to absorb the maximum possible energy, which is about 220 J.

The above results indicate that at least two similar 4 kA pulses can be accelerated in the α-cavity. If we assume that the pulses are timed to absorb maximum energy, then based on the Eq. 2, the second, third and fourth pulses would have energy gains approximately

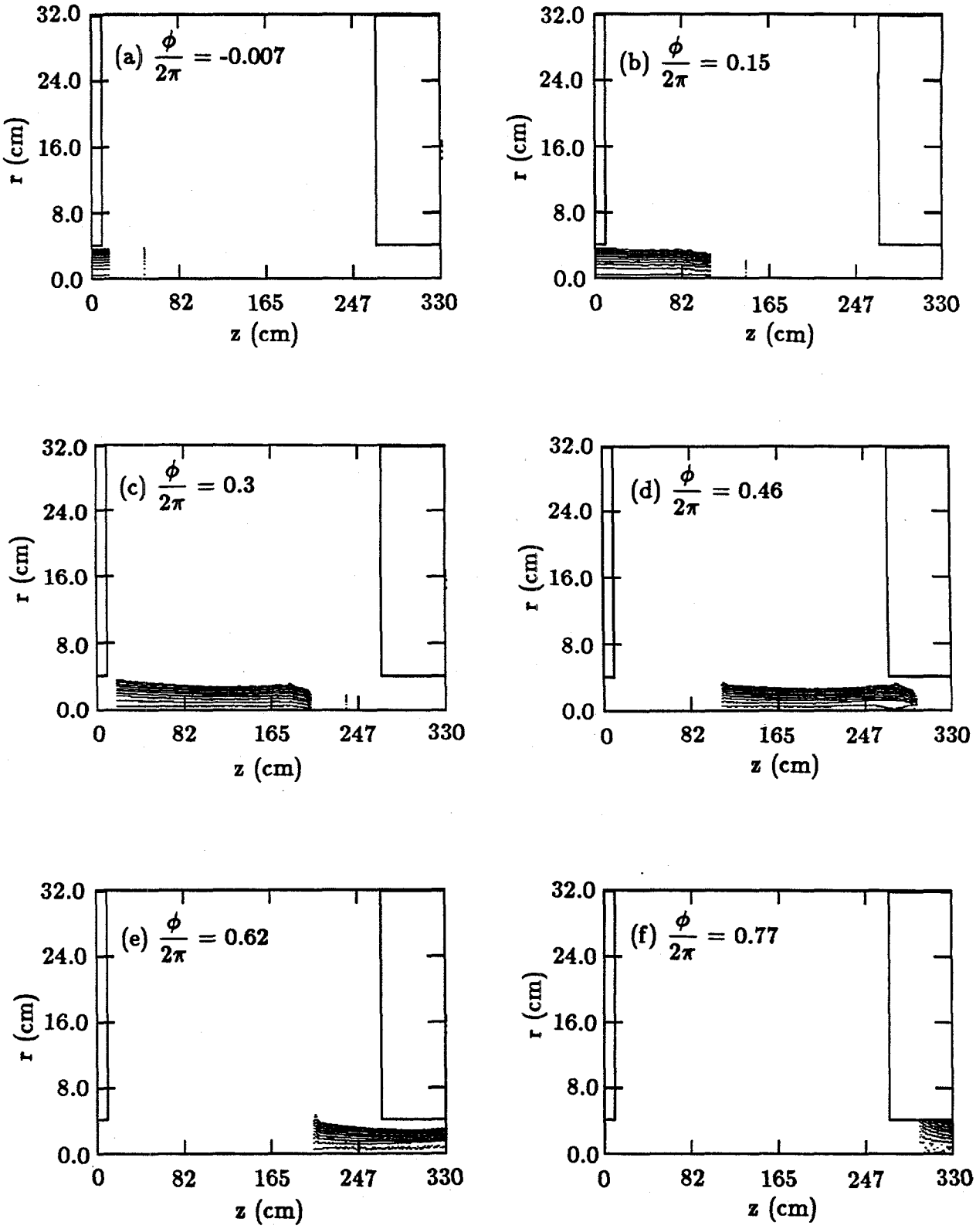

Figure 13. Particle plots over two rf periods of chopped injection of 4 MV, 4 kA beam into PHERMEX α-cavity. (Run AE1).

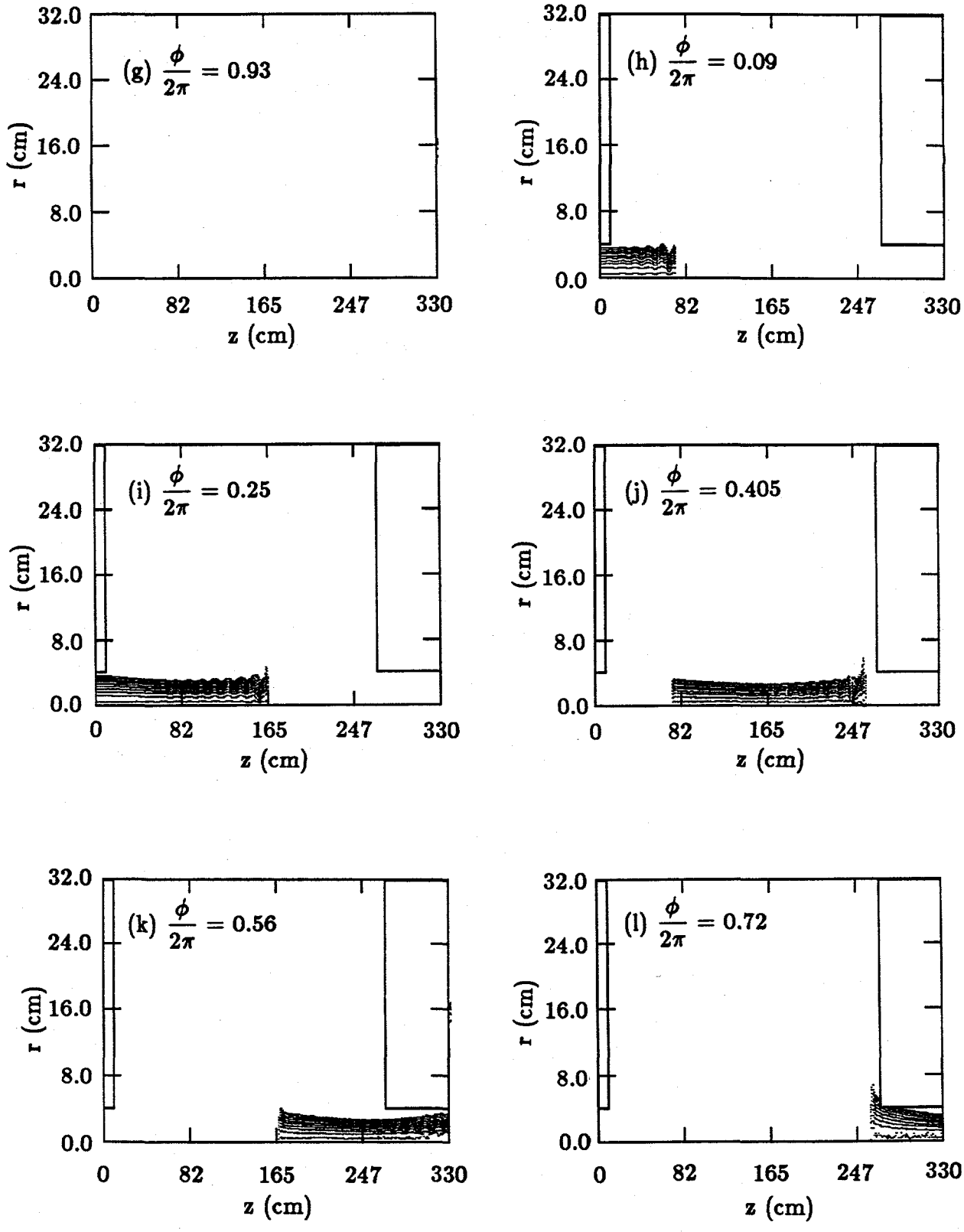

Figure 13. Concluded.

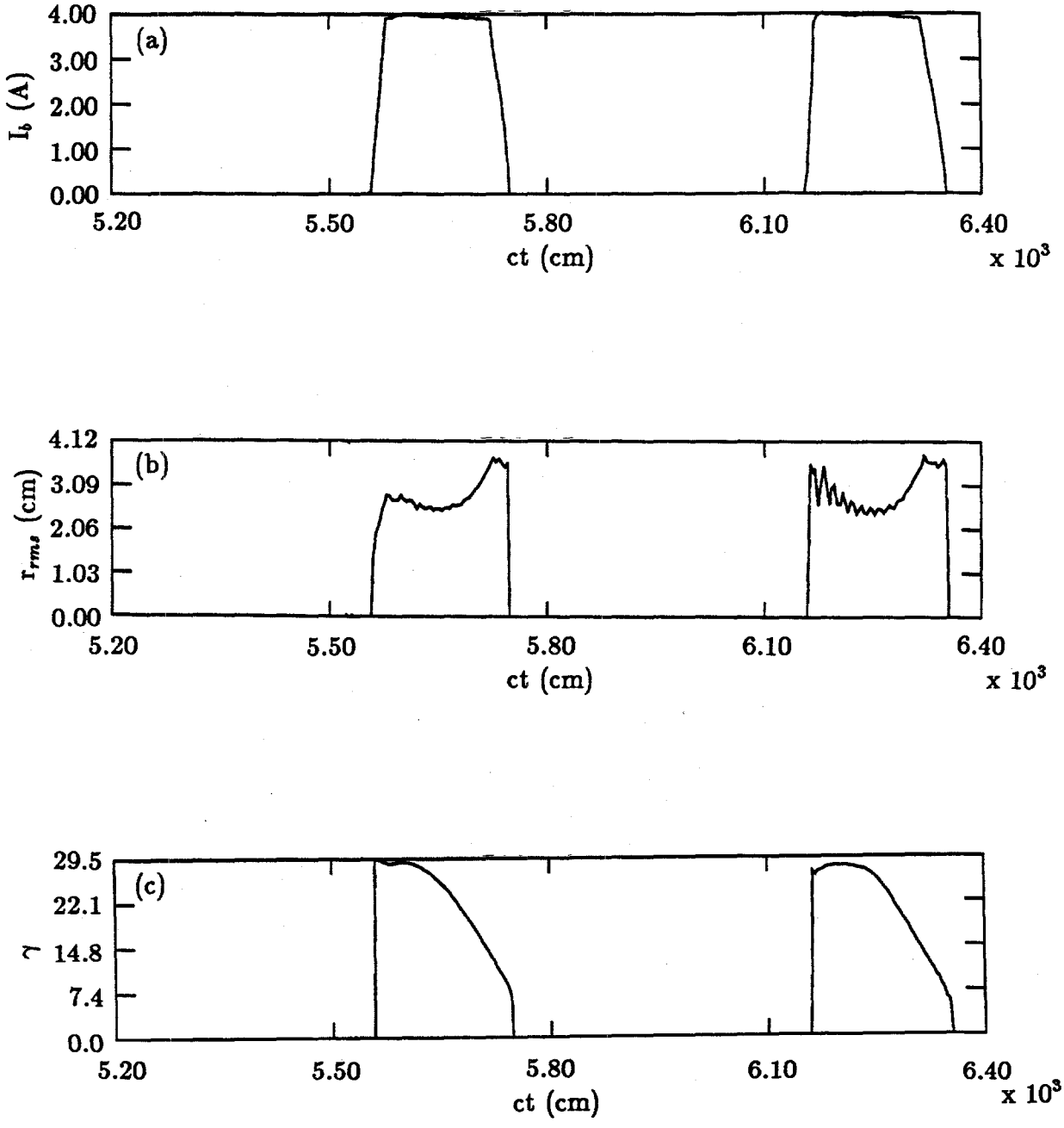

Figure 14. Time histories of (a) beam current, (b) *rms* radius and (c) energy (γ) at the exit of the α cavity for chopped beam injection. (Run AE1).

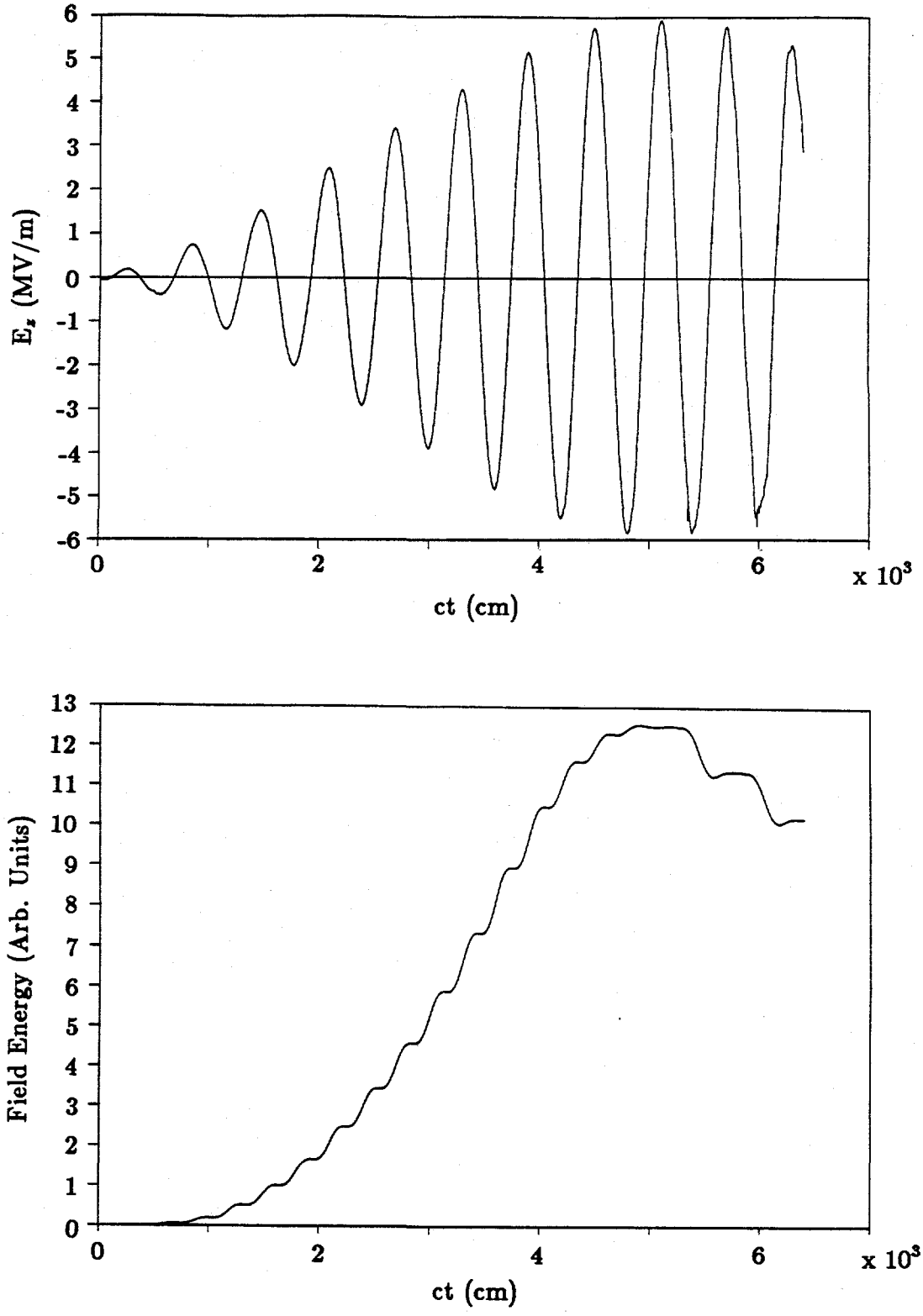

Figure 15. Time histories of (a) axial electric field in center of cavity and (b) cavity field energy for chopped beam injection. (Run AE1).

94%, 87%, 80%, of the first pulse, respectively. It would be straightforward to extend the simulations to check these estimates. It is also possible to take the particles exiting the α-cavity and inject them into subsequent cavities. This would provide an accurate estimate of transport efficiency and energy dispersion at the end of the accelerator.

While these results show that it is may be possible to accelerate a 4 kA beam in PHERMEX, at this point we do not consider this an optimal strategy for increasing the machine dose. This is because of the concomitant requirement for a costly high-voltage injector. With current technology, the pulse length of such an injector is limited to $\leq$100 ns. Thus, one can accelerate only 4–5 pulses. By upgrading the present 500 A injector to one producing 1–1.5 kA (cf. Sec. 2) for 200 ns, one can potentially increase the machine dose by 2–3 times. In addition, a low-voltage injector may permit use of a photometal cathode[4,5] to produce a chopped pulse train for synchronous injection. At present, there is no way to provide this type of emission control for a high-voltage cold cathode.

4.0 REX CALCULATIONS

4.1 Simulation of Dipole Beam Motion in REX Diode

The transverse oscillations observed on streak records of the REX beam are believed to be caused by electromagnetic dipole modes in the diode cavity.[6] Experimental cold-test measurements and calculations using URMELT[7] have found modes near the observed dominant frequency of 240 MHz. This frequency corresponds to a rough estimate of the lowest *TM* mode of the diode cavity.[6*] In order to model the effect of a dipole mode on the beam, we carried out a simulation of the diode cavity using the 3-D PIC code IVORY. (The 2-D version of ISIS normally used to model the diode cannot treat this intrinsically 3-D problem.) The geometry used is shown in Fig. 16. A beam is generated by launching a symmetric *TEM* wave from the open left boundary. Space-charge-limited emission takes place off a specified area of the cathode. An anode magnet focuses the beam to prevent it hitting the drift-tube wall. To excite a dipole mode in the cavity, an oscillating 240 MHz radial dipole current is driven along the left boundary. A vector plot of the magnetic field generated is shown in Fig. 16b. We see the *TM* character of the field in the AK gap. The amplitude of the transverse magnetic field is about 4.9 gauss near the $r = 0$ axis and the cathode surface. The effect of this field on the beam centroid is shown in Figs. 17 and 18. We see from Fig. 17b that the amplitude of the oscillations 64 cm downstream of the diode is $\approx \pm 3$ mm. Since the dipole mode is plane-polarized, the beam motion is also. The anode magnet just rotates the plane of polarization.

The experimentally measured oscillation amplitude is on the order of 0.1 cm. Scaling the above results, this implies oscillating magnetic fields on the order of 1–2 gauss in the AK gap.

4.2 Effect of Iron Rings in Anode Magnet on Beam Emittance

The solenoids for the DARHT accelerator contain iron rings with diameters slightly smaller than the diameter of the windings. The purpose of the rings is to improve the

---

*The *TM* cutoff frequency of a coax with an inner conductor radius of 25 cm and an outer conductor radius of 85 cm is 262 MHz.

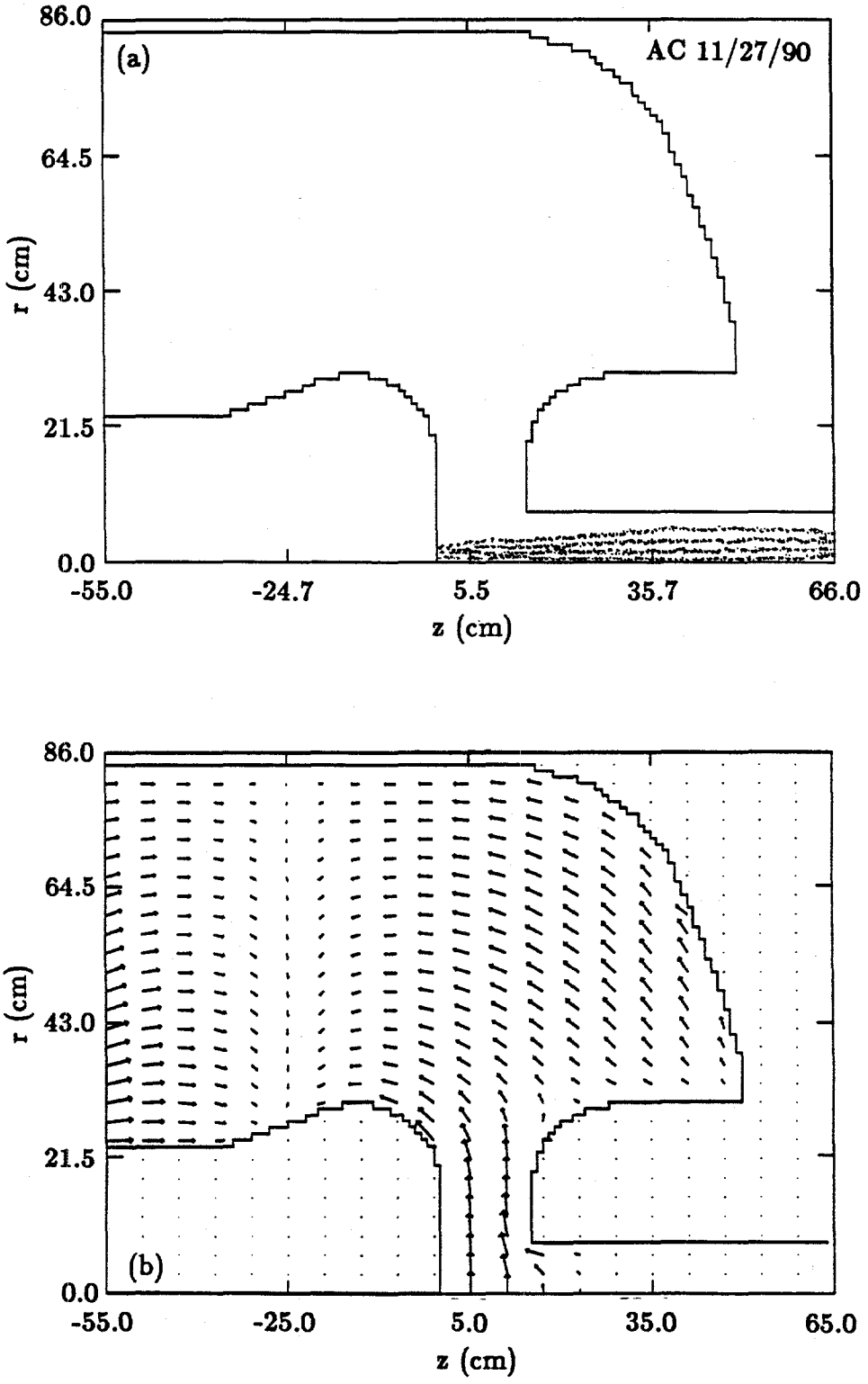

Figure 16. IVORY simulation of dipole beam motion in REX. Particle plot is shown in (a), and magnetic field vector plot is shown in (b). (Run AC).

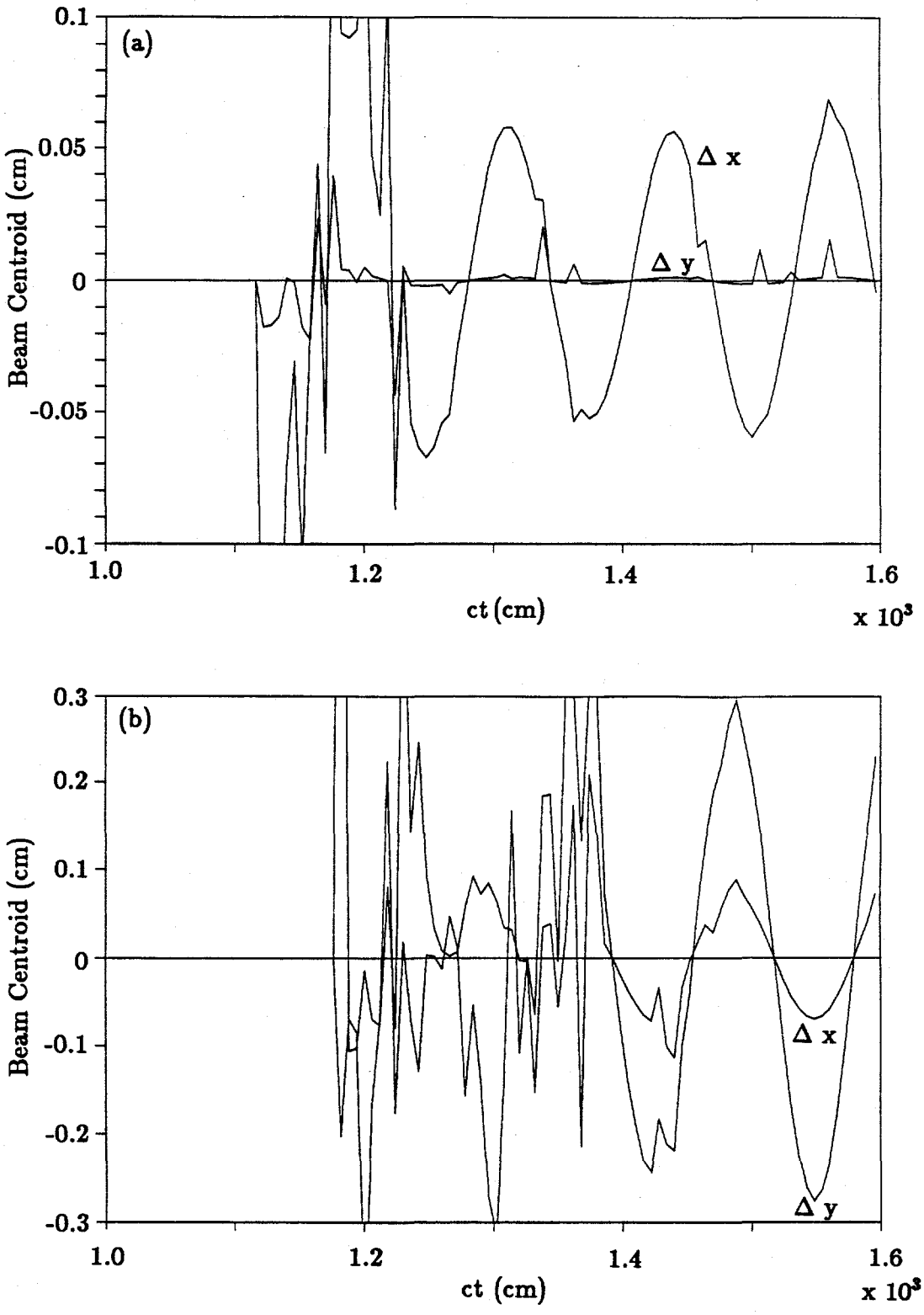

Figure 17. Time history of beam centroid displacement at (a) 14 cm and (b) 64 cm from cathode surface. The initial noise is from the low-energy head of the beam. (Run AC).

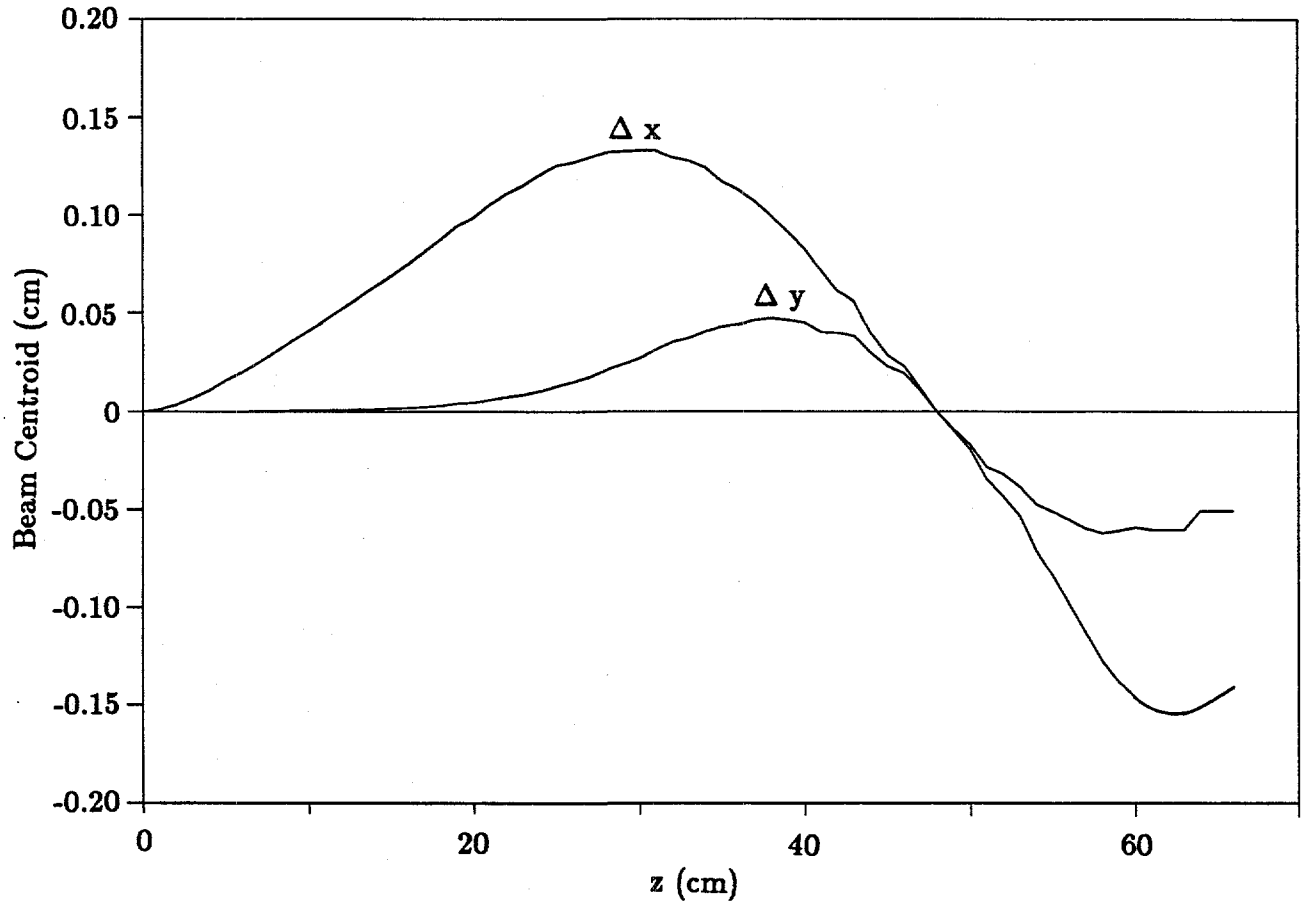

Figure 18. Snapshot of beam centroid displacement vs. z at $ct = 1560$ cm. Cathode surface is at $z = 0$. (Run AC).

cylindrical symmetry of the magnetic field. Since considerable effort has gone into the design and testing of these solenoids, it is desirable to use a similar design for the anode magnet. The iron rings obviously cause some ripple in the axial field, so a simulation was performed to see if this affects the beam emittance. Dimensions for the iron-ring magnet together with those for the iron-free magnet used in previous simulations are given in Table 3.

TABLE 3. Dimensions of Iron and Iron-Free Anode Magnets

	Iron	Iron-Free
Coil Dimensions (cm) :		
Inner radius	9.47	8.26
Outer radius	10.82	10.95
Length	48.46	48.26
Ring Dimensions (cm) :		
Inner radius	8.476	
Outer radius	9.112	
Length	0.636	

The code POISSON[2] was used to model the iron-ring magnet. The public version of the code did not allow sufficient resolution of the nine 0.25-in × 0.25-in rings, so a large-dimension version was obtained from Mary Menzel.[8] The POISSON geometry and output are shown in Fig. 19. The midplane symmetry of the magnet was used to reduce the size of the calculation. The field generated by POISSON was used to carry out the ISIS simulation in Fig. 20. The magnet strength is such that beam is almost parallel as it exits the field, as shown in Fig. 20a. The cathode temperature was set to zero, so that the emittance in Fig. 20b is due solely to nonlinear external and self fields. We see that the normalized Lapostolle emittance downstream of the magnet is approximately 0.037 cm-rad. The nominal cathode temperature obtained from experiments is in the range of 60–130 eV, which gives a normalized emittance of 0.08–0.12 cm-rad.[6] The emittances due to nonlinear forces and cathode temperature do not add in any simple way. However, from the results of previous simulations (see, e.g. Figs. 1–4 of Ref. 9), the contribution of the emittance in

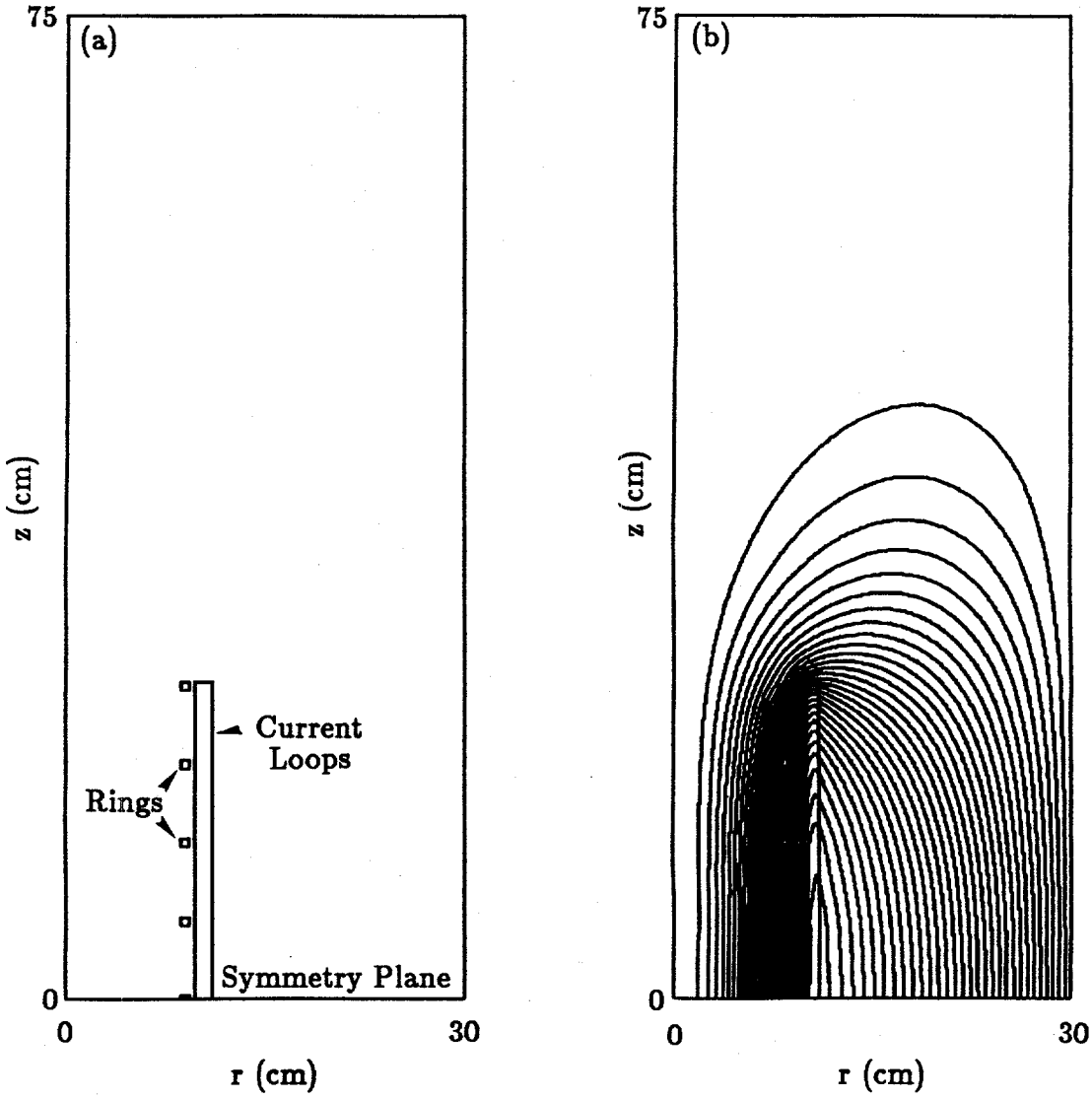

Figure 19. POISSON calculation of magnetic field of iron-ring anode magnet. Coil and ring positions are shown in (a), and magnetic field-line plot is shown in (b).

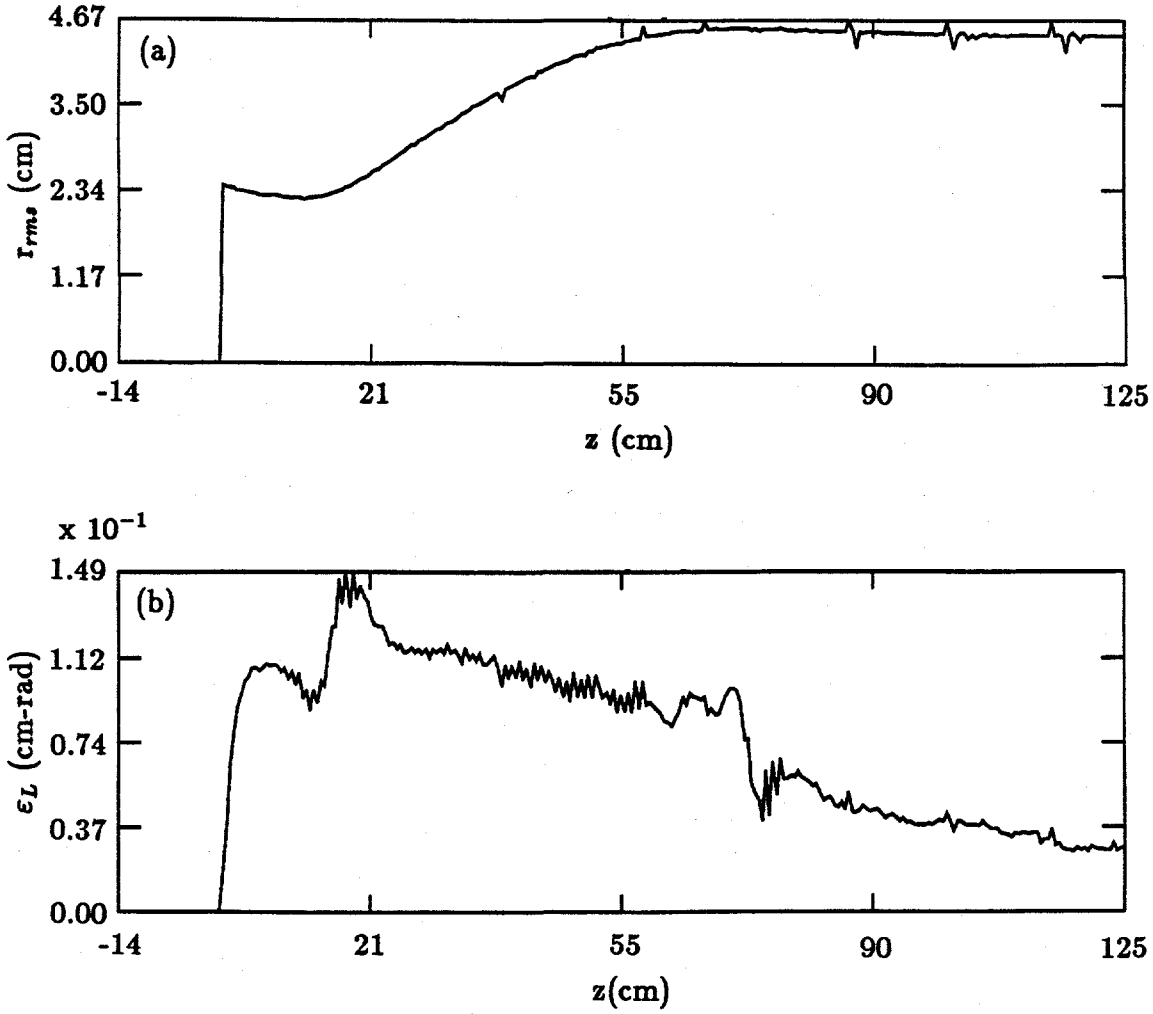

Figure 20. Results of ISIS diode simulation results using POISSON field in Fig. 19, showing (a) *rms* radius and (b) normalized emittance vs. z. (Run IX, 09/18/90).

Fig. 20b to the total emittance will be small compared to the contribution of the cathode temperature.

Our conclusion is that the use of the iron-ring magnet will not cause can any significant degradation of the expected beam emittance.

4.3 Injection of REX Beam into a Plasma Channel

Partially ionized gases can be used as an alternative to magnetic fields to focus and transport high-current beams. Some simulations were carried out to investigate the use of a plasma lens to focus the REX beam to a small spot. One way to create such a lens is to ionize low-pressure benzene using a KrF laser, as described in Ref. 10. In this reference, a benzene vapor pressure near 1 μm was used, corresponding to a number density of about 3×10^{13} cm^{-3}. Ionization fractions of 10^{-4}–10^{-3} were measured.

The goal of the simulations was to focus the beam to a spot approximately 50 cm from the center of the anode magnet, and to look at the effect of a plasma on the spot-size. The simulations were carried out in two parts. First, the beam was generated in the diode and transported through the anode magnet in vacuum, as shown in Fig. 21. The magnetic field strength is $\int B_z^2 dz \approx 39$ kG^2-cm, which brings the beam to a focus at $z = 107$ cm when no plasma is present, as shown in Fig. 22a. In Figs. 22b and 22c, we show the effect of plasma channels with ion densities, n_i, of 2.8×10^{10} cm^{-3} and 1.78×10^{11} cm^{-3}, respectively. For the 1 μm pressure cited above, these densities correspond to ionization fractions of 9×10^{-4} and 6×10^{-3}, respectively. The channel has a radius of 1.27 cm, and extends over the length of the simulation region in Fig. 22. The channel is modeled by immobile ions and neutralizing electrons. The ratio of the line density of channel electrons to beam electrons, denoted by f, is 0.016 for the case in Fig. 22b, and 1.0 for Fig. 22c. Thus, in both cases, all the channel electrons are expelled as the beam enters, leaving the positive ions. The effect on the minimum focal spot is shown in Fig. 23. For $n_i = 0$, 2.8×10^{10} cm^{-3}, and 1.78×10^{11} cm^{-3}, we see that 80% of the charge is inside radii of 0.16, 0.11 and 0.055 cm, respectively. In each case, the normalized beam emittance is approximately constant at 0.12 cm-rad through the focus.

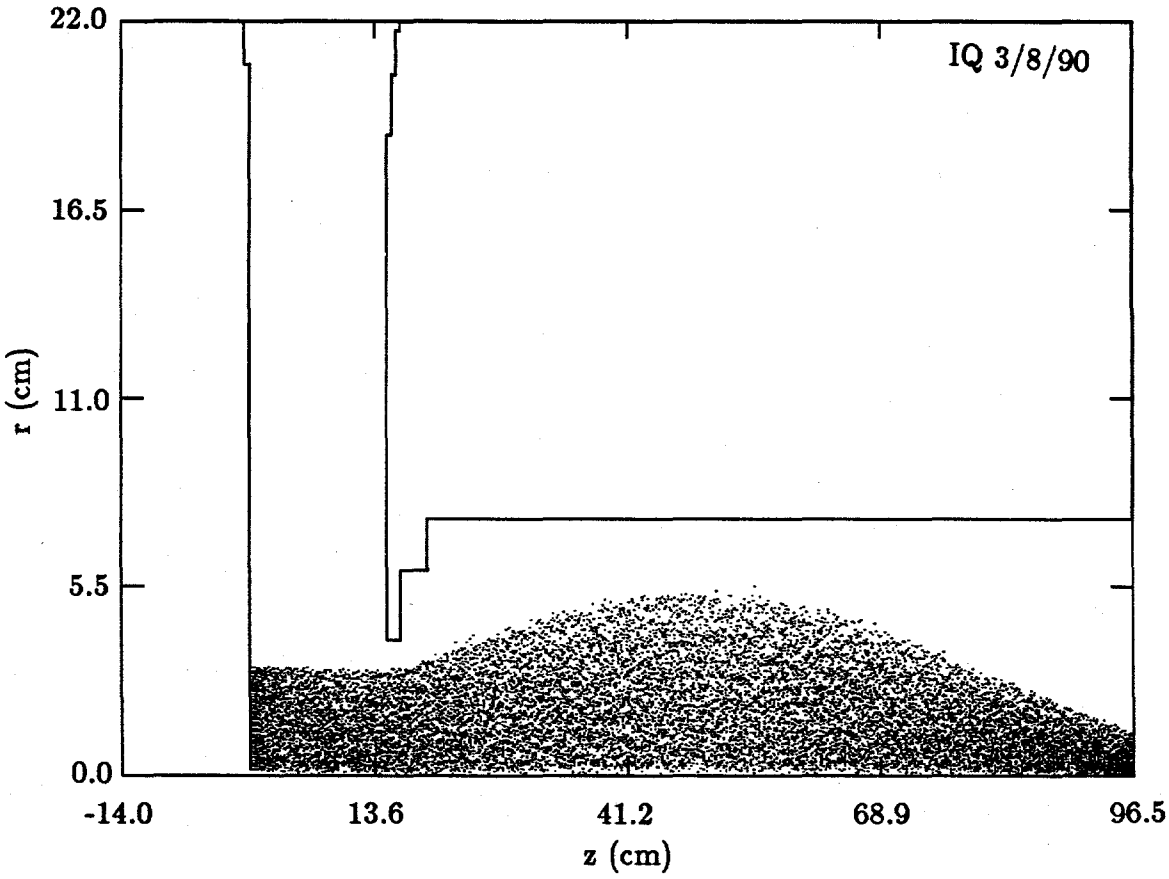

Figure 21. Beam transport prior to injection into a plasma channel. (Run IQ).

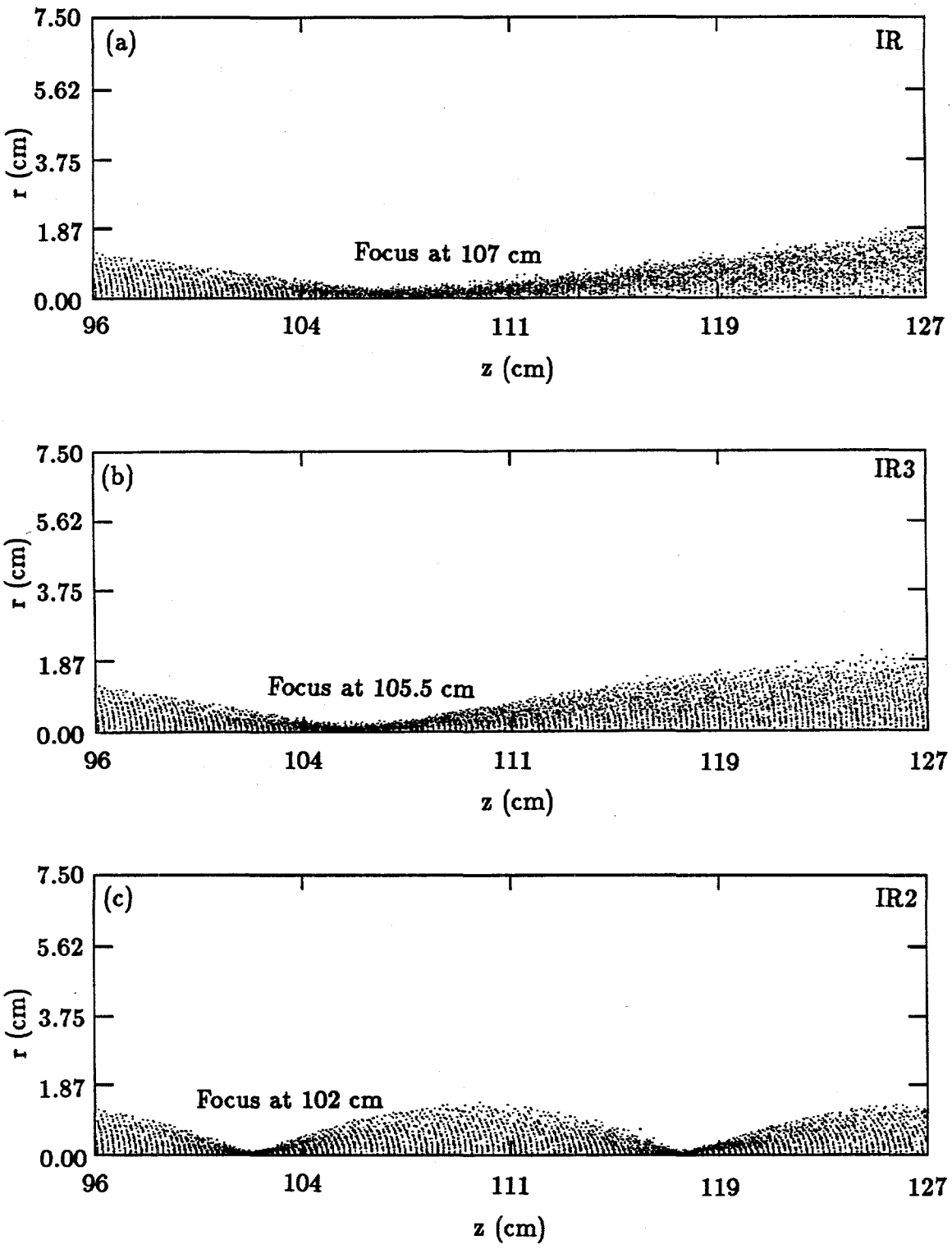

Figure 22. Continuation of simulation in Fig. 21 with (a) no channel, and channels with (b) ion density $= 2.8 \times 10^{10}$, (c) ion density $= 1.78 \times 10^{11}$. (Runs IR, IR3, IR2).

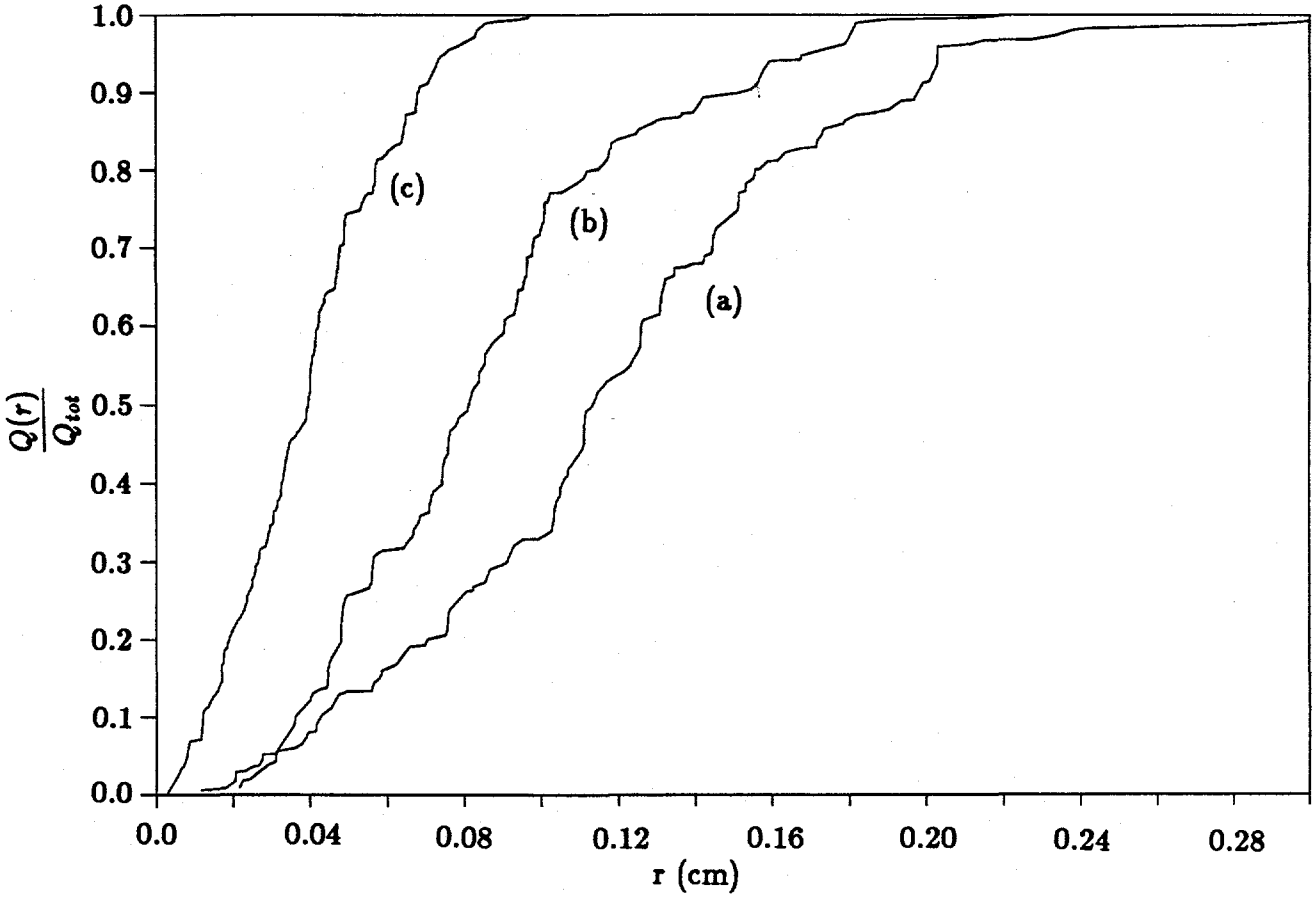

Figure 23. Ratio of integrated charge density to total charge plotted vs. r at the minimum focal spot for the three cases in Fig. 22.

5.0 LASER BACK-SCATTERING OFF AN ELECTRON BEAM

XUV (10–100 nm) and soft X-ray (1–10 nm) light sources are of interest in the manufacture of integrated circuits and for instrument calibration. One way to generate radiation in this regime is by backscattering laser light off a relativistic electron beam. This method of producing high-energy photons was proposed in both the United States and the Soviet Union soon after the invention of lasers.[9,10] The phenomenon has been used as an electron beam diagnostic.[11] Backscattering experiments using high-power lasers have been carried out in Japan[12] with the eventual goal of producing stimulated emission, i.e. an X-ray FEL. The laser and electron beam requirements for stimulated emission are very taxing, however. We have carried out some preliminary calculations to see whether, by using intense electron beams and high-power lasers, one can generate doses of practical interest with single-particle, spontaneous emission.

We start by computing the scattering cross-section for a single electron. In the frame co-moving with the electron, one can treat the interaction between the laser and electron simply as classical Thomson scattering provided $\gamma\hbar\omega_0 \ll mc^2$, where γ is the lab-frame electron energy, ω_0 is the frequency of the incident laser light, and m is the electron mass. For the 4 MV ($\gamma \approx 8.8$) REX beam and a 10.6 μm (0.117 eV) CO_2 laser, this inequality is easily satisfied. In the beam frame, the differential cross-section is

$$\frac{d\sigma}{d\Omega'} = \frac{1}{2} r_0^2 \left(1 + \cos^2\theta'\right) \tag{3}$$

where r_0 is the classical electron radius, and $\pi - \theta'$ is the angle between the incident and scattered photons. We see that the radiation pattern is symmetric in the forward and backward directions. Transforming back to the laboratory frame, we find that, for $\gamma \gg 1$, Eq. 3 becomes

$$\frac{d\sigma}{d\Omega} \approx \frac{4r_0^2\gamma^2\left(1+\gamma^4\theta^4\right)}{\left(1+\gamma^2\theta^2\right)^4} \tag{4}$$

where now the pattern is strongly peaked in the direction of the electron beam, and falls off rapidly for $\theta > 1/\gamma$. The total cross-section, which is Lorentz invariant, is obtained from Eq. 3 to be $\sigma_0 = (8\pi/3)r_0^2$, i.e. the Thomson cross-section. From Eq. 4, we find that

half the scattered photons are in the $1/\gamma$ cone. The frequency of the scattered photons is related to the incident photon frequency by

$$\omega_s \approx \frac{4\gamma^2\omega_0}{1+\gamma^2\theta^2} = \begin{cases} 4\gamma^2\omega_0 & \text{at} \quad \theta = 0 \\ 2\gamma^2\omega_0 & \text{at} \quad \theta = 1/\gamma \end{cases} \tag{5}$$

The peak photon energy is thus $4\gamma^2\omega_0 = 36$ eV (34 nm), which is in the middle of the XUV spectrum, for the REX beam. Multiplying Eq. 4 by Eq. 5 and integrating over θ, we find that 78% of the radiated energy is in the $1/\gamma$ cone. In addition, we find that the average photon in the $1/\gamma$ cone has 78% of the peak photon energy. Using the latter, we can compute the energy radiated from an interaction region of length L and radius R in which we have a photon density n_l and an electron density n_e for a time τ:

$$E = \left(0.78 \times 4\gamma^2\hbar\omega_0\right)\left(0.5\sigma_0\right)\left(2n_l c\right)\left(\pi R^2 L n_e\right)\tau \tag{6}$$

where the first term in parentheses is the average photon energy in the $1/\gamma$ cone, the second is the cross-section for scatter into the $1/\gamma$ cone, the third is the photon flux density relative to the moving electrons, and the fourth is the number of electrons. In terms of the laser power, S (watts), and beam current I_b (A), Eq. 6 becomes

$$E = 1.4 \times 10^{-22}\gamma^2 S I_b L\tau/R^2 \quad \text{millijoules} \tag{7}$$

where τ is measured in ns and L, R are in cm.

To estimate the x-ray energy obtainable from the REX machine, we use the parameters in Table 4. The useful interaction length between the electron beam and the laser is diffraction-limited by the Rayleigh length of the laser light, given by

$$Z_l = \pi a_0^2/\lambda_0 \tag{8}$$

where a_0 is the radius of the focal spot and λ_0 is the wavelength of the laser. If we take $a_0 = 2.5$ mm, and an interaction length $L = Z_l = 185$ cm, then Eq. 7 gives 0.16 mJ.

TABLE 4. Nominal parameters for REX X-ray source

Beam Current	5 kA
Beam Energy	4 MV
Pulse Duration	50 ns (flat-top)
Laser Energy	1 kJ
Laser Wavelength	10.6 μm
Pulse Duration	50 ns

To get into the X-ray regime with a CO_2 laser, one needs a beam energy of at least 8 MV. Since only a tiny fraction of the beam and laser energy is converted into hard photons, the ability to recirculate the beam and laser would greatly increase the efficiency of this scheme. Beam recirculation presents the greatest technical difficulty. It may be possible to adapt the fast kicker and septum magnets proposed for synchrotron radiation sources.[13] Fast magnets are also being investigated at Sandia for the Recirculating Linear Accelerator.

In the near future, we hope to perform some initial experiments using the REX beam and a CO_2 laser. The experiments will measure the distribution of scattered radiation, and characterize the effects of beam emittance, focusing magnetic fields, finite source extent and other non-ideal factors.

6.0 REFERENCES

1. D. Venable, D. O. Dickman, J. N. Hardwick, E. D. Bush, Jr., R. W. Taylor, T. J. Boyd, J. R. Ruhe, E. J. Schneider, B. T. Rogers, and H. G. Worstell, "PHERMEX: A Pulsed High-Energy Radiographic Machine Emitting X-Rays," LA-3241, Los Alamos Scientific Laboratory, 1967.

2. M. T. Menzel and H. K. Stokes, "User's Guide for the POISSON/SUPERFISH Group of Codes," LA-UR-87-115, Los Alamos National Laboratory, January 1987.

3. D. Mitrovich, "A Model For Calculating PHERMEX Performance," AMRC-R-661, Mission Research Corporation, December 1984.

4. T. J. Kauppila, L. A. Builta, J. K. Crutcher, J. C. Elliot, and D. C. Moir, "A Pulsed Electron Injector Using A Photocathode Irradiated By An Excimer Laser," *1987 IEEE Particle Accelerator Conference* (IEEE Cat. No. 87CH2387-9) p. 273.

5. J. D. Saunders, T. J. Ringler, L. A. Builta, T. J. Kauppila, D. C. Moir, and S. W. Downey, "Simple Laser-Driven Metal Photocathodes As Cold High-Current Electron Sources," *1987 IEEE Particle Accelerator Conference* (IEEE Cat. No. 87CH2387-9) p. 337.

6. T. P. Hughes, R. L. Carlson, and D. C. Moir, "High Brightness Electron Beam Generation and Transport," *J. Appl. Phys.* **68**, 2562 (1990).

7. P. Allison, private communication.

8. M. Menzel, private communication.

9. T. Hughes, R. M. Clark, R. L. Carlson, L. A. Builta, T. J. Kauppila, D. C. Moir, and R. N. Ridlon, "Diode and Transport Calculations for REX, DARHT, and PHERMEX," MRC/ABQ-R-1244, Mission Research Corporation, February 1990.

10. R. L. Carlson, S. W. Downey, and D. C. Moir, "Guiding of an electron beam from an RF accelerator by a laser-ionized channel," *J. Appl. Phys.* **61**, 12 (1987).

11. R. H. Milburn, "Electron Scattering by an Intense Photon Field," *Phys. Rev. Lett.* **10**, 75 (1963).

12. F. R. Arutyunyan and V. A. Tumanyan, "The Compton Effect on Relativistic Electrons and the Possibility of Producing Beams of Hard γ Rays," *JETP*, **44**, 2100 (1963).

13. S. C. Chen and T. C. Marshall, "Thomson Backscattering from a Relativistic Electron Beam as a Diagnostic for Parallel Velocity Spread," *Phys. Rev. Lett.* **52**, 425 (1984).

14. K. Mima, Y. Kitagawa, T. Akiba, K. Imasaki, S. Kuruma, H. Ohigashi, S. Miyamoto, S. Fujita, S. Nakayama, Y. Tsunawaki, H. Motz, T. Taguchi, S. Nakai, and C. Yamanaka, "Experiment and Theory on CO_2 Laser Powered Wiggler and Induction Linac FEL," *Nuc. Inst. Meth.* **A272**, 106 (1988).

15. F. C. Younger, A. Jackson, K. D. Jenkins, P. F. Meads, and L. S. B. Ng, "Electron Storage Ring For X-Ray Lithography," *Proc. 1987 Particle Accelerator Conference* (IEEE Cat. 87CH2387-9) p. 440.